METHOD DEVELOPMENT OF COMPOUND SPECIFIC ISOTOPE RATIO MEASUREMENT OF METHYLMERCURY IN SEDIMENT BY MULTICOLLECTOR - ICP - MS

A Thesis Submitted to the Committee on Graduate Studies in Partial Fulfillment of the Requirements for the Degree of Master of Science in the Faculty of Arts and Science

TRENT UNIVERSITY

Peterborough, Ontario, Canada
© Copyright by Adelheid Willsie 2025
Environmental & Life Sciences M.Sc. Graduate Program
January 2025

Abstract

Method Development of Compound Specific Isotope Ratio Measurement of Methylmercury in Sediment by Multicollector - ICP - MS

Adelheid Willsie

This work presents a new online method using gas chromatography coupled to the multicollector-inductively coupled plasma-mass spectrometer for methylmercury (MMHg) isotope ratio measurement. An extraction method using distillation was developed that effectively extracted MMHg from up to 5 grams of sediment, imparting no isotope fractionation on MMHg during extraction. Isotope ratios from transient signals were calculated using three different data treatment approaches, facilitated by a data processing application, IsoCor. Peak Area Integration using 80% of the peak gave the most accurate and precise results. Using the proposed methodology, an external precision (2 SD) of ± 0.59‰ for NIST 3177 was measured. This method can be applied to samples with MMHg concentration as low as 0.1 ng/g and was successfully applied to real sediment samples however, additional research to improve the precision of the method is required for the detection of small differences between samples.

Key Words: methylmercury, isotope ratio measurement, MC-ICP-MS, compound specific isotopic ratios

Acknowledgements

There are a few very important people who, one way or another, had a considerable impact on me during my master's. To everyone who has helped me during the last two years, I would like to express my heartfelt gratitude.

First and foremost, I'd like to say a special thank you to my supervisor Dr. Holger Hintelmann. Thank you for sparking my interest in mercury research, if not for you reaching out about my application to the program, I'd likely have spent two years counting microplastics through a microscope. You always treated my questions as valid and fully explained concepts even when they weren't relevant to my research. I'm very thankful for the opportunity to participate in three field sampling opportunities and two international conferences. Thank you for imparting me with a fraction of your vast knowledge that extends well beyond just mercury research.

My profound thanks go to Zhengwen Zhou. Your help with the MC-ICP-MS was crucial to my success in my master's. If not for your help, I'm not sure I would have ever successfully measured accurate isotope ratios. Thank you for always asking how my lab work was going and being willing to drop everything to help me in the WQC for hours when things weren't working.

I would like to thank Beatriz Martins for her unwavering support during her visits to Canada. I very much appreciate the discussions we had puzzling over lab issues, and general conversations about life. Bia, our weekend (and sometimes during the week) adventures will always be a good memory.

Thank you, Erin, your support during the last two years has been so greatly appreciated. Having someone who was also in grad school to commiserate with kept me going. Thank you for listening to countless hours of me explaining the many problems and setbacks I experienced during my master's and for celebrating my successes.

Throughout my whole university experience, my sister Janoah has provided support only a sister could. She is solely responsible for the correct use of commas in this document. I'm sure you know how much I appreciate you without having to express it here. Many thanks to my parents. Although they both have no idea what I really did in my master's, my mom would still call to ask how things were going with "my machine". Mom and Dad, your support is appreciated.

Finally, I would like to thank all the lab members I had the pleasure of meeting during my time in the Hintelmann Lab, even those who were here for only a short time. Both teaching others and being taught, helped me develop as a scientist. Meeting so many international scientists was not what I expected from my master's, but it was an experience for which I am grateful.

Table of Contents

List of Figures

List of Tables

List of Abbreviations

ADME	Atmospheric mercury deposition event
CV	Cold Vapour
CVAFS	Cold Vapour Atomic Fluorescence Spectroscopy
GC	Gas Chromatography
Hg(0)	Elemental Mercury
Hg(II)	Oxidized Mercury
LRS	Linear Regression Slope (Isotope ratio calculation method)
MC-ICP-MC Spectrometer	Multicollector-Inductively Coupled Plasma-Mass
MDF	Mass Dependent Fractionation
MIF	Mass Independent Fractionation
MMHg	Methylmercury
NIST	National Institute of Standards and Technology
PAI	Peak Area Integration (Isotope ratio calculation method)
PBP	Point-By-Point (Isotope ratio calculation method)
SD	Standard Deviation
THg	Total Mercury

Chapter 1: Introduction

1.1. General Introduction

Mercury is a global pollutant and toxic contaminant that poses a serious risk to human health (Kumar, 2024). It is classified as a transition metal in the d-block on the periodic table and is the only metallic element that is liquid at standard temperature and pressure. It is a ubiquitous, naturally occurring element that does not degrade in the environment (Gworek et al., 2020). The most toxic effects of mercury are generally attributed to its organic form, methylmercury (MMHg) (Hong et al., 2012). MMHg primarily affects the central nervous system. Once ingested, it rapidly penetrates and damages the blood-brain barrier, impairing its function (Chang, 1977). All forms of mercury can be transported through the blood-placental barrier disrupting brain development of a fetus, which is why mercury exposure is a great concern for pregnant women (Tong et al., 2021).

Mercury can be released into the environment from both natural and anthropogenic sources. Natural sources of mercury consist of both primary emission sources and re-emission of previously deposited mercury. Natural sources account for almost 70% of the global mercury emission budget (AMAP Assessment 2021: Mercury in the Arctic, 2021). Primary sources include volcanic emissions, geothermal sources, and weathering of the earth's crust. Mercury is re-emitted generally from vegetation, land surfaces and water surfaces (R. Mason & Pirrone, 2009). The largest contributor to natural mercury emissions is the ocean, which contributes 52% of the global emissions due to natural sources. In decreasing order of magnitude, other significant natural emission sources are biomass burning (13%), re-emission from tundra and grasslands

(9%), re-emission from forests (7%), and volcanoes and geothermal sources (2%) (Pirrone et al., 2010). Since the end of the Industrial Revolution in 1840, the anthropogenic emissions have increased dramatically. Depending on the country, the current anthropogenic emissions are 10 to 63 times higher than before the Industrial Revolution (Li et al., 2020). The major anthropogenic contributors are fossil fuel power plants, artisanal small-scale gold mining, non-ferrous metals manufacturing, cement production, waste disposal, and caustic soda production (AMAP Assessment 2021: Mercury in the Arctic, 2021).

In response to concerns surrounding the continual increase in anthropogenic emission of mercury, a global treaty was negotiated and was entered into force in August 2017 (Eriksen & Perrez, 2014). It is known as the Minamata Convention on Mercury, named after a catastrophic contamination of MMHg disposed in wastewater in Minamata, Japan starting in the 1950s, which caused mercury poisoning, coined Minamata disease, in thousands of individuals (Kessler, 2013). Today, the main avenue of human exposure to mercury is through fish and seafood consumption (Hong et al., 2012). Because of this, health organizations publish recommendations for fish consumption to limit ingestion of mercury compounds (Vieira et al., 2015). Considerable scientific investigation has been conducted on mercury to understand its sources, cycling through the environment, avenues of human exposure and impacts on environmental and human health (Gworek et al., 2020). This information is needed to develop regulatory methods to lower emissions and limit human exposure to mercury. Efforts to learn more about mercury are ongoing, and new methods continue to be introduced to further our understanding of mercury in the environment.

1.2. Mercury in the Environment

The biogeochemical cycling of mercury through its different chemical forms and different environmental compartments is known as the mercury cycle (Selin, 2009). In the environment, mercury exists in two main oxidation states, as elemental mercury Hg(0), and as oxidized mercury Hg(II) (Whalin et al., 2007). The most common organic forms of mercury are methylated mercury compounds, namely monomethylmercury (MMHg) and dimethylmercury (West et al., 2023). Dimethylmercury exists primarily in the deep ocean, where there are low oxygen regions (Black et al., 2009; R. P. Mason & Fitzgerald, 1993). Mercury exists in the atmosphere, in oceans, lakes, rivers and other bodies of water, in soil and sediment, in vegetation, and in animals. MMHg has a strong affinity for sulphur-containing compounds such as the amino acid cysteine, resulting in MMHg bioaccumulating in organisms (Thera et al., 2022). MMHg also biomagnifies through food chains, leading to very high MMHg concentrations in top predators (Clayden et al., 2013; G. Liu et al., 2012).

Mercury in the atmosphere is either elemental mercury, Hg(0), or divalent mercury, Hg(II) (Lindberg & Stratton, 1998). The predominant species, accounting for at least 95% of the mercury in the atmosphere, is elemental mercury (Stein et al., 1996), which is characterized by relatively low deposition velocity and high vapor pressure at ambient conditions (G. Liu et al., 2012). Mercury is removed from the atmosphere by both wet and dry deposition (Miller et al., 2005). Hg(0) has a long residence time in the atmosphere of 0.5 – 1 year, allowing long range transport of Hg(0) to locations far from its emission (R. Mason & Pirrone, 2009). Hg(II) can be removed rapidly from the atmosphere via deposition (Miller et al., 2005). In comparison, Hg(0) generally must

undergo oxidation to Hg(II) to be subject to deposition and therefore removal from the atmosphere (G. Liu et al., 2012).

In water, the most prevalent mercury form is Hg(II), which has high solubility in water and readily binds to ligands such as chloride, bromide or dissolved organic matter (Ignatavičius et al., 2022). MMHg is also present in water and can be demethylated by photochemical reactions (Barkay & Gu, 2022), which is a rather significant process (Sellers et al., 2001), accounting for considerable losses of MMHg in water. Mercury can enter aquatic environments through atmospheric deposition, direct discharge, and runoff or erosion of contaminated soil (Acquavita et al., 2021). In water, Hg(II) can be photochemically or biologically reduced to Hg(0) (Kritee et al., 2008). Hg(0) has limited solubility in water and therefore can be volatilized into the atmosphere. This process is facilitated by both natural factors such as tidal currents, wind, waves, and storms, and anthropogenic factors such as dredging, trawling, and other fishing activities, and is a significant source of re-emission of mercury to the atmosphere (Bettoso et al., 2023).

Once in the water column, mercury can accumulate in sediment due to simple sedimentation (Ignatavičius et al., 2022). Sediment can act as either a sink or source of mercury depending on the environmental conditions. Mercury can be remobilized into the water column, acting as a source of mercury, or a sink if additional sedimentation removes mercury from being able to exchange with the water (Stein et al., 1996). In sediment, the predominant mercury species are Hg(II) and MMHg. The particle characteristics of the sediment, such as mineral composition and quality of clay, affect mercury sorption and therefore the concentration of mercury in sediment (Ignatavičius et al., 2022). Organic matter has a high affinity for Hg(II), therefore highly organic

sediments are often linked with high mercury concentrations (O'Connor et al., 2019). Most mercury in sediment is bound to organic matter such as humic acids, but it can also be associated with inorganic components of sediment such as sulphides or other metal oxides (O'Connor et al., 2019).

The competing processes of mercury methylation and MMHg demethylation result in a steady state concentration of MMHg (Ignatavičius et al., 2022). Methylation occurs when Hg(II) is converted to methylated mercury species, which is most pertinently MMHg (G. Liu et al., 2012). Methylation and demethylation generally occur in aquatic environments and is facilitated by both biological and abiotic processes (Ignatavičius et al., 2022). Biotic methylation is mediated by bacteria, mainly sulphate reducing and iron reducing bacteria, and is believed to be the main avenue of methylation. Many factors affect the rate of methylation including temperature, pH, redox potentials, availability of nutrients and electron acceptors, as well as the presence of ligands and adsorbing surfaces (G. Liu et al., 2012). Methylation is increased in low pH environments. It is proposed that the low pH provides increased protons that are able to undergo cation exchange to liberate Hg(II) from complexes, making the Hg(II) available for methylation (Stein et al., 1996). Increased temperatures have also been demonstrated to increase MMHg production (Z. Yang et al., 2016). Abiotic methylation is responsible for a much smaller amount of methylation. Abiotic methylation is proposed to occur in the presence of methylcobalamin, methyltin compounds, and humic matter (Weber, 1993).

Demethylation of MMHg also occurs by biological and abiotic processes (Barkay & Gu, 2022). Microbial degradation of MMHg occurs by either a reductive or oxidative

pathway. In the oxidative process, both methane and carbon dioxide are produced and in the reductive process, only methane is produced (G. Liu et al., 2012). Reductive demethylation is mediated by organomercury lyase, an enzyme that is encoded by mercury resistance *(mer)* operon (Schaefer et al., 2004). It has been demonstrated to be the predominant demethylation pathway in contaminated soils (Marvin-DiPasquale et al., 2000). Oxidative demethylation is carried out by mainly sulphate reducers and methanogens (Oremland et al., 1991) and occurs in soils with lower MMHg concentrations (Marvin-DiPasquale et al., 2000). Abiotic demethylation is caused primarily by photochemical degradation (G. Liu et al., 2012). The rate of degradation is dependant on the radiation intensity and the wavelength of light. Dark abiotic demethylation has also been observed but this mechanisms of demethylation are not fully understood (Barkay & Gu, 2022).

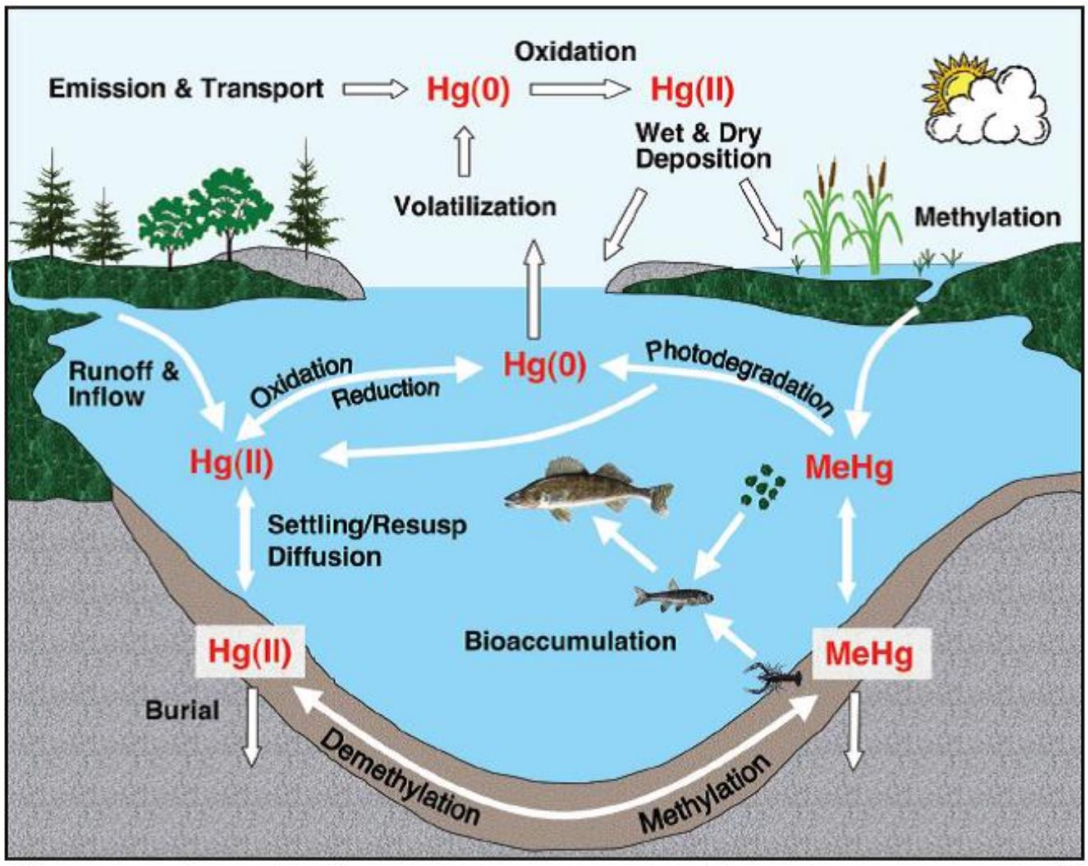

Figure 1.1. Diagram of mercury cycling in the environment (adapted from Engstrom, 2007).

1.3. Mercury in the Arctic

The arctic, although very remote, is not free from mercury contamination. A major route of mercury transport to the arctic is through the atmosphere (AMAP Assessment 2021: Mercury in the Arctic, 2021). Because Hg(0) has such a long residence time in the atmosphere, it is subject to long-range transport to remote locations. This long-range transport brings atmospheric emissions from populated, industrial, southern latitudes to the arctic. Atmospheric winds deliver mercury to the arctic at all times of the year (Macdonald et al., 2000). In winter, northern Eurasian sources are predominantly transported and in summer, transport is dominated by mid latitude Asian and North American sources (Durnford et al., 2010). In the atmosphere, Hg(0) is oxidized to Hg(II),

which has a short atmospheric residency time and is deposited on landscapes below. Deposition of mercury in the arctic is enhanced by a phenomenon called atmospheric mercury depletion events (AMDEs) (Kirk et al., 2012). This occurs during the spring in the arctic when the physical and chemical conditions promote the oxidation of Hg(0) and its deposition as Hg(II), resulting in an unexpected low concentration of Hg(0) in the air. ADMEs require Hg in the atmosphere, cold temperatures, a stable inversion layer, sunlight, and reactive halogens (Steffen et al., 2008).

Ocean currents and river discharge are another major route of mercury transport to the arctic (Kirk et al., 2012). Ocean transport is a much slower process than atmospheric transfer and can take many years to travel from emission source to the Arctic Ocean. Waters enter the Arctic Ocean from the North Atlantic via the Fram Straight and the Barents Sea and from the North Pacific from the Bering Straight (AMAP Assessment 2021: Mercury in the Arctic, 2021). Major rivers bringing inland waters to the Arctic Ocean include the Mackenzie and Yukon Rivers in the Canadian arctic, and the Ob, Yenisei and Lena Rivers in Asia (Kirk et al., 2012; Paffrath et al., 2021).

With the increased global temperatures that earth is experiencing due to climate change, the potential for significant permafrost thaw has become a grave concern (Sutherland et al., 2019). Two recent studies were conducted on mercury in permafrost and estimated the Hg pool in the top 100 cm of boreal and Arctic soils range from 408 Gg (Olson et al., 2018) to 863 Gg (Schuster et al., 2018). In the entire Northern hemisphere permafrost region, Schuster et al. (2018), estimate an Hg pool of 1656 Gg, which is nearly twice the amount of mercury stored in the soil, atmosphere and oceans combined.

The consequences of permafrost thaw are already being observed. When ice-rich permafrost thaws, it can form a depression in the earth, creating a relatively small and shallow lake called a thermokarst lake (Borge et al., 2017). Thermokarst lakes have been observed to have high rates of methylation, which is concerning, as it would suggest that the permafrost thaw is creating methylation hotspots; however the literature is still limited (Lehnherr, St. Louis, Emmerton, et al., 2012; Lehnherr, St. Louis, & Kirk, 2012; Tarbier et al., 2021). Hammerschmidt et al. (2006) suggest that increased temperatures in the arctic may enhance methylation in tundra and lake sediments and reduce photodecomposition. The melting permafrost will expose northern populations to the toxic mercury that is released, posing a serious risk to their health (Schuster et al., 2018). Because permafrost is a large sink of mercury and there is a concern of increased rates of methylation with warming temperatures, research on mercury in the arctic is of great importance.

1.4. Mercury Isotope Ratio Analysis

Mercury has seven stable isotopes with the following natural relative abundance: ^{196}Hg (0.15%), ^{198}Hg (9.96%), ^{199}Hg (16.87%), ^{200}Hg (23.10%), ^{201}Hg (13.18%), ^{202}Hg (29.86%), ^{204}Hg (6.87%) (Zadnik et al., 1989). Isotopes are atoms with the same atomic number (same number of protons) but different number of neutrons, which causes them to have different atomic masses. The difference in masses can be a cause for isotope fractionation, which is changes in the relative abundance of isotopes in reaction products compared to the initial reactants, when mercury undergoes different chemical or physical transformations like evaporation or methylation (Evans et al., 2001). Because mercury has no naturally occurring radiogenic isotopes, any isotope variation must be the result of

fractionation processes (Hintelmann, 2012). With the development of the multicollector-inductively coupled plasma-mass spectrometer (MC-ICP-MS), the precision of measuring isotope ratios of heavier elements has dramatically improved so that even the small but distinct differences in mercury isotope abundances can be precisely measured (Blum & Bergquist, 2007). The magnitude of fractionation is small, reported as per-mil (‰) (Hintelmann, 2012). Fractionation can be either mass dependent (MDF), represented as δ, meaning it scales linearly with mass or mass independent (MIF), represented as Δ (L. Zhang et al., 2022). There are four different mechanisms used to explain mercury fractionation. These mechanisms are equilibrium isotope effects, kinetic isotope effects, nuclear volume effects, and magnetic isotope effects (**Figure 1.2**).

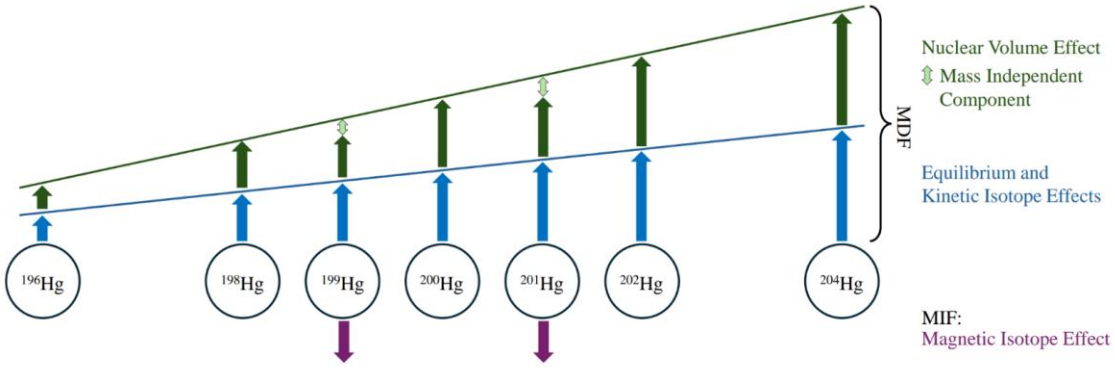

Figure 1.2. Qualitative diagram of the influence of fractionation effects on Hg isotope system. MDF consists of equilibrium and kinetic isotope effects as well as nuclear volume effects. MIF caused by anomalies in linear scaling of nuclear volumes, and magnetic isotope effects (adapted from Wiederhold et al., 2010).

Equilibrium isotope fractionation is attributed to the differences in the energy of the vibrational frequencies of compounds in a system at equilibrium (Wiederhold, 2015). Equilibrium occurs when the rate of the forward and reverse reactions is equal, resulting in unchanging concentrations of the reactants and products. The energy of vibrational

frequencies is affected by the atomic mass of atoms in the bond (Hintelmann & Zheng, 2011). Bonds with isotopes of lower atomic masses are associated with higher vibrational frequencies, so heavy isotopes tend to be incorporated into bonds preferentially to lower the zero-point energy of the bond (Wiederhold et al., 2010). The heavy isotopes are preferentially enriched in substances in which the element is bound by the "stiffest" bonds (i.e. bonds with the highest force constants). Bond stiffness is affected by factors such as bond length, oxidation state, coordination number, and electronic configuration (Wiederhold, 2015). The fractionation caused by equilibrium isotope effects are generally small and decreases with increasing temperatures because the difference in energy between isotopes diminishes at higher temperatures (Wiederhold, 2015).

Kinetic isotope fractionation is driven by the different reaction rates of compounds containing heavy and light isotopes and is only preserved in incomplete processes (Schauble, 2004). This is because during complete processes, all the reactants are transformed into products, resulting in isotope ratios of the products that are identical to the original reactants and the kinetic isotope effects are concealed. Types of processes associated with kinetic effects include evaporation, diffusion, dissociation reactions, and biologically mediated reactions (Wiederhold, 2015). During kinetic processes, isotopic exchange is limited by an energy barrier known as the activation energy. Bonds involving light isotopes require less activation energy to break due to their smaller disassociation energies, which results in the light isotopes being enriched in the products (Schauble, 2004). The impact of kinetics effects on the isotopic composition of a sample is strongly dependent on how far the reaction has advanced. Often, Rayleigh models are used to describe the progression of isotope ratios during a reaction and can be especially useful in

determining the extent of transformations of a specific process based on the isotope ratios (Wiederhold, 2015). Generally, the greatest fractionation due to kinetic effects is observed in the remaining reactants, which become enriched in heavy isotopes (Hintelmann & Zheng, 2011).

Nuclear volume effects, also known as nuclear field shift effects, occur due to differences in the volume and shape of isotope nuclei (Zheng & Hintelmann, 2010). The magnitude of nuclear volume effects increases with increasing atomic number, so although the effect is minute for light elements, it is an essential explanation of fractionation in heavy elements like mercury (Wiederhold, 2015). Nuclear size and charge distribution change between different isotopes because of the different numbers of neutrons. This causes each isotope to have a slightly different electrostatic field acting on the s orbital's electrons (Hintelmann & Zheng, 2011). Light isotopes, compared to heavy isotopes, have a smaller size and larger nuclear charge distribution, resulting in a lower ground state electron energy. To achieve the lowest energy of the system, compounds with the smallest number of s electrons are preferentially enriched in heavy isotopes (Bigeleisen, 1996). Most fractionation caused by nuclear volume effects does scale linearly with mass, however there is a small part of the effect that can lead to MIF. This is due to small differences in the expected nuclear volume of the odd mass isotopes. Both atomic radii and mass increase with increasing number of neutrons, however, it is not a perfectly linear relationship. The odd isotopes (^{199}Hg and ^{201}Hg) have a smaller radius than the linear trend would suggest (Wiederhold, 2015).

Magnetic isotope effects are kinetic effects that only affects the odd mass isotopes (^{199}Hg and ^{201}Hg) and has been shown to cause large mass-independent fractionation

(Wiederhold, 2015). This fractionation occurs in reactions that produce a radical pair intermediate. It is the recombination of these radical pairs that can cause MIF (Hintelmann & Zheng, 2011). If the radical pair come together in a triplet state, where the unpaired electrons have parallel spins, then the recombination of the pair is spin-forbidden. However, the odd isotopes (^{199}Hg and ^{201}Hg), which have non-zero nuclear spins and a magnetic moment, can undergo a fast triplet-singlet conversion, allowing for the recombination to the original reactant (Wiederhold, 2015). In comparison, the non-magnetic isotopes undergo a much slower triplet-singlet conversion, which leads to the enrichment of the even, non-magnetic isotopes in the reaction products, and the odd isotopes in the starting reactant (Hintelmann & Zheng, 2011).

Recently, significant MIF of even isotopes has been observed, mainly in atmospheric samples (Chen et al., 2012; Demers et al., 2013; Yuan et al., 2015). The mechanism of fractionation is not yet fully understood (Cai & Chen, 2016).

Mercury isotope ratios are measured using a gas-liquid separator to create a continuous cold vapour flow of mercury. The sample is continually mixed with stannous chloride as it enters the gas-liquid separator, known as a cold vapour system (CV), and the stannous chloride reduces the mercury in the samples to Hg(0). A gas flow is used to sweep the Hg(0) from solution and into the torch (Hintelmann, 2012). ICP-MS instruments have an inherent mass bias that arises when ions of different masses are transmitted through the mass spectrometer with different efficiencies, resulting in non-uniform instrument sensitivity across the mass range and therefore inaccurate isotope ratios (Ingle et al., 2003; L. Yang & Sturgeon, 2003). For mercury analysis, thallium is most commonly used as an external mass bias correction. The National Institute of

Standards and Technology produces a thallium reference material with a certified $^{205/203}$Tl ratio (NIST 997). The thallium is introduced either through a desolvation unit or a spray chamber to produce a thallium vapour that is mixed with the mercury gas before entering the torch (Blum & Johnson, 2017). The Russel equation is used for mass bias correction (Russell et al., 1978):

$$R^{obs} = R^{true} \cdot \left(\frac{m_2}{m_1}\right)^f \quad (1)$$

Where R^{obs} is the measured ratio, R^{true} is the corrected ratio, m_1 and m_2 are the masses of the isotopes of interest used in R and f is the mass bias factor. The mass bias factor is calculated using the measured thallium ratio and certified $^{205/203}$Tl ratio. Then the mass bias factor is used to correct the measured mercury ratios. Rather than calculating the measured isotope ratios, results are commonly reported as a deviation from an agreed upon standard (Hintelmann, 2012), which is the NIST 3133 standard for the mercury isotope system. All unknown samples are bracketed with 3133 before and after the measurement and the values are reported as the difference in isotope ratios between the sample and the average of the bracketing standard, using delta notation:

$$\delta^{xxx}Hg = \left(\frac{\left(\frac{^{xxx}Hg}{^{198}Hg}\right)_{sample}}{\left(\frac{^{xxx}Hg}{^{198}Hg}\right)_{NIST\ 3133}} - 1 \right) \times 1000 \quad (2)$$

Where xxx represents the mercury isotope of interest. The standard concentration should be within 10% of the sample concentration to ensure concentration is not impacting the measured ratios. MIF is reported using the capital delta (Δ^{xxx}Hg) as the difference

between the measured $\delta^{xxx}Hg$ and the predicted value assuming only MDF (using $\delta^{202}Hg$ for reference) according to the following equations (Blum & Bergquist, 2007):

$$\Delta^{199}Hg = \delta^{199}Hg - (\delta^{202}Hg \times 0.2520) \quad (3)$$

$$\Delta^{200}Hg = \delta^{200}Hg - (\delta^{202}Hg \times 0.5024) \quad (4)$$

$$\Delta^{201}Hg = \delta^{201}Hg - (\delta^{202}Hg \times 0.7520) \quad (5)$$

$$\Delta^{204}Hg = \delta^{204}Hg - (\delta^{202}Hg \times 1.4930) \quad (6)$$

Mercury isotope ratio analysis can be used for both source and process tracing (L. Zhang et al., 2022). For source tracing, the isotope ratios of sources and receptors must differ significantly from each other (C. Feng et al., 2019; X. Feng et al., 2010; Gray et al., 2015). Source tracing can be used for both natural and contaminated systems, but natural systems are more challenging because i) the isotopic signature of the mixing sources may not be sufficiently distinct, ii) more than two sources may contribute the total found in the sample, and iii) fractionation processes can affect the isotopic signatures (Wiederhold, 2015). When mercury undergoes a transformation, it causes a shift in the isotopic signature which is reflected in the residual mercury pool. Specific transformations and their effect on isotopic signatures have been investigated in laboratory studies. A few examples of this include photoreduction of Hg(II) (Bergquist & Blum, 2007; Zheng & Hintelmann, 2009), microbial reduction of Hg(II) (Bettoso et al., 2023; Kritee et al., 2008), and dark abiotic reduction of Hg(II) (Wang et al., 2021; Zheng & Hintelmann, 2010). But there are still many processes that require additional study (M. T.-K. Tsui et al., 2020).

1.5. Previous Studies on Mercury Isotope Fractionation

The field of mercury isotope ratio analysis started to develop in the early 2000s. Now, almost 25 years later, there are a vast number of studies being published every year. These studies measure the isotope ratio of all mercury forms present in a sample and fall into three general categories: (1) Laboratory studies of fractionation during biotic and abiotic chemical transformation of mercury, (2) Measurement of environmental samples to investigate biogeochemical transformations that occur, and (3) Measurement of environmental samples to "fingerprint" point sources of Hg (Blum, 2011). Now that the protocols and methods are well established and the method is reliably applied to analyse isotope ratios of the total Hg present in real environmental samples, interest has turned to measuring isotope ratios of MMHg. Recent studies on MMHg isotope ratios have demonstrated that the isotopic signature of inorganic mercury can be distinctly different than that of MMHg (Donovan et al., 2016; Janssen et al., 2015; Perrot et al., 2016; Poulin et al., 2021; Qin et al., 2018, 2020; M. T. K. Tsui et al., 2012), meaning the total mercury isotopic signature cannot be used to investigate the transformation of MMHg. Being the most toxic and bio-accumulative form of mercury, investigation into MMHg sources, pathways for formation, and biological uptake is of great interest and importance (Blum & Johnson, 2017).

Two main challenges must be overcome to analyse the isotope composition of MMHg. First, MMHg must be extracted and purified from the sample matrix (Blum & Johnson, 2017). An appropriate extraction method is one that does not impart any fractionation to the sample (L. Zhang et al., 2022). This is most easily ensured by having a quantitative extraction method. Many extraction methods are not 100% specific to

MMHg, meaning they may also extract other forms of mercury in a sample, requiring additional purification steps to isolate MMHg (Blum & Johnson, 2017). Isolation of MMHg has generally been accomplished offline through solvent extraction (Masbou et al., 2013; Qin et al., 2018), anion exchange resin separation (Crowther et al., 2023; Poulin et al., 2021; Rosera et al., 2020), two-step purge and trap (W. Zhang et al., 2021) and distillation (Dzurko et al., 2009; Janssen et al., 2015; Rosera et al., 2020), or through instrumental techniques using gas chromatography (GC) (L. Zhang et al., 2022). Non-chromatographic, methodology defined speciation protocols analyse MMHg isotope ratios by first oxidizing MMHg to inorganic Hg followed by $SnCl_2$ reduction. Chromatographic techniques can either be online, meaning the GC is coupled directly to the MC-ICP-MS, or offline, where the GC is used for separation of MMHg from other forms of mercury, then the MMHg fraction is collected in a trapping solution before analysing the isolated MMHg by $SnCl_2$ reduction (L. Zhang et al., 2022).

The second challenge is the mass of MMHg needs to be sufficient to achieve a signal that will result in reliable isotope ratio measurements (Janssen et al., 2015). This can be an added challenge with samples that have low MMHg content, like sediments. The MMHg in sediments generally only accounts for ~1% of all mercury forms in the sample, meaning a large quantity of sediment is required to extract sufficient MMHg for an isotope ratio measurement (Janssen et al., 2015). In comparison to concentration measurements, which generally only require a few picograms of MMHg, Dzurko et al. (2009) found that more than 2 ng of MMHg was required to produce a satisfactory response on the MC-ICP-MS. Because of this restriction, many methods have been applicable only to contaminated samples that have high concentrations of MMHg.

The first offline method proposed by Masbou, Point, and Sonke (2013) for MMHg isotope ratio analysis was a two-step extraction/back extraction method used to isolate MMHg. Acidic sodium bromide, cupric sulphate, and toluene was used to extract mercury from the sample, then the toluene phase was transferred to a falcon tube containing sodium thiosulphate, and the MMHg was back extracted into the aqueous phase. Following extraction, the sample was analysed using CV-MC-ICP-MS. The method was applied to measure the MMHg isotope signature of seven certified reference materials and the external precision of replicate measurements was within 0.12‰ (2 SD). Janssen et al. (2015) developed an extraction method for sediment using distillation to extract mercury species. The samples were ethylated and purged onto a Tenax® trap before subsequent introduction to a GC column. A solenoid valve at the end of the GC column was used to direct the MMHg peak onto a gold bead trap. Finally, the trapped MMHg was desorbed into an oxidizing solution. This method had an external precision of 0.15‰ (2 SD). Qin et al. (2018) adapted the purge and trap method from Janssen et al. (2015) and used a HNO_3 leaching solvent extraction to analyse MMHg isotope ratios in paddy soils. Rosera et al. (2020) proposed an extraction using distillation, followed by an anion-exchange resin separation to isolate MMHg, with an external precision of 0.15‰ (2 SD). One final study by Zhang et al. (2021) developed a two-step purge and trap method that achieved a precision of 0.15‰.

The conventional method of analysing isotope ratios by MC-ICP-MS involves a steady, constant flow of the sample into the instrument. This creates a stable signal that is measured by the instrument for each sample. When coupling a GC column to the MC-ICP-MS, the instrument will no longer receive a stable signal, instead it will receive a

transient signal that will change as the species of interest leave the GC column. Evans et al. (2001) were the first to measure mercury using transient signals. In the analysis of coal samples, the samples were preconcentrated onto gold traps. They were then thermally desorbed into the plasma, resulting in a transient signal. The isotope ratios changed over the peak, so the integration of the whole peak was used to calculate the isotope ratios. Xie et al. (2005) added to this method by developing a sample introduction method that extended the peak width, improving the precision. Krupp and Donard (2005) investigated the drift in isotope ratios during peak elusion, a frequent observation when recording transient signals irrespective of the analyte. They eliminated chromatographic fractionation, analyte concentration, and changes in instrument mass bias as a source of the drift. They found that peak width influences the extent of drift, suggesting that the drift was due to the change in intensity with time.

Epov et al. (2008) was the first to measure species specific isotope ratios using GC coupled to a MC-ICP-MS. They used an isothermal temperature program to extend the peak width to at least 30 – 60 seconds. With injections of ~500 pg of sample, the peak height was between 0.5 – 1 V. This method had an external precision of 0.56‰ (2 SD). Dzurko et al. (2009) also developed a method to analyse transient signals of MMHg. Using 2 ng injections to the GC, the peak signal intensity was ~2 V. They evaluated three different methods of calculating the isotope ratios. First was peak area integration, in which the isotope ratios were determined by using the integrated area under the peak for each isotope. The second method was point-by-point, where the isotope ratio is calculated at each integration time point and averaged across the peak. The final method was the peak apex method, where only the highest signal of the peak is used to calculate the ratio.

Using the point-by-point method, the precision was 0.47‰ (2 SD). They were also able to determine that the peak drift occurred due to the Faraday detectors not being able to respond quickly enough to the fast-changing signal. Rodríguez-González et al. (2012) was the first to study environmental samples using the method developed previously (Epov et al., 2008). They investigated the fractionation of mercury during methylation by anaerobic bacteria under dark conditions.

Epov et al. (2010) investigated different methods for calculating isotope ratios from transient signals. They introduced and validated a new method called linear regression slope for mercury isotope ratio calculation based on the method published by Fietzke et al. (2008). This method is based on a linear regression analysis using the slope of the plotted transient intensities of ^{198}Hg vs. the isotope of interest to determine the isotope ratio. The method was shown to be superior to previous methods of calculating ratios and had good precision, 0.2 – 0.5‰ (2 SD). The method developed by Epov et al. (2008) was used by Jiménez-Moreno et al. (2013), Perrot et al. (2015), and (2016) to investigate the fractionation of MMHg caused by different environmental processes. Bouchet et al. (2018) developed a method for analysis of samples with very low concentrations using an online preconcentration strategy. They used a packed liner that the sample was injected into to concentrate the sample before subsequently entering the GC. Finally, Queipo-Abad et al. (2019) evaluated different parameters that effect the accuracy and precision of compound specific isotope ratio measurements. They evaluated the effect of peak width, integration time, acquisition points, and different data treatment strategies. They found that the ideal parameters were narrow peaks of 2 – 5 secs,

0.131 sec integration time, 321 – 641 acquisition points, and the use of the linear regression method for isotope ratio calculations.

1.6. Research Gaps and Study Objectives

There is a great incentive to study the fate of MMHg as it is the most toxic form of mercury that poses a serious risk to human health. Isotope ratio analysis of total mercury (THg) in a sample proved very helpful in investigating mercury transformation, but up until now, most of the research has not been able to study species specific isotope ratios, which overlooks a vital part of mercury cycling (L. Zhang et al., 2022). The analysis of MMHg isotope ratios has been limited by the lack of analytical methods to isolate MMHg from samples. The method defined strategies present several disadvantages in comparison to online analysis methods including time consuming and labour-intensive analysis methods. The methods are generally limited to contaminated samples with high concentrations of mercury species and often require additional pre-concentration steps prior to analysis (Epov et al., 2012). The traditional analysis of mercury isotope ratios can take several minutes and requires concentrations of at least 1 ng/mL to achieve adequate signal, meaning that at least 10 ng of the mercury species of interest is required. In comparison, online GC methods concentrate the sample into a transient peak, requiring significantly less MMHg to achieve signal response similar to the intensity achieved using the traditional set up. For these reasons, online GC is an appealing option particularly because of its separation power, and its straightforward analysis.

The approach of this research is to couple a GC (Tekran® Model 2700 Automatic Methylmercury Analysis System) to the MC-ICP-MS for the online measurement of

isotope fractionation of MMHg. The Tekran® 2700 has previously been coupled with a quadrupole ICP-MS in many applications (Bento & Hintelmann, 2024; Bussan et al., 2022; Štrok et al., 2019). The Tekran® 2700 effectively separates the Hg(0), Hg(II), and MMHg within a sample and would allow characterization of the isotope fractionation of multiple species within one sample. The Tekran® 2700 results in mercury species peaks with base widths of ~30 sec, which based on previous studies, should be appropriate for isotope ratio analysis (Epov et al., 2008).

The objectives of this research were first to develop a method to isolate MMHg from sediment samples that does not cause fractionation and is compatible with analysis by GC. The second objective was to interface the GC with the MC-ICP-MS and develop a method to analyse MMHg isotope ratios. This included both establishing the physical coupling between the GC and the MC-ICP-MS, as well as developing a data processing strategy to calculate the MMHg isotope ratios. This research will establish a method that can be used to examine MMHg transformations in the environment.

Chapter 2: Materials and Methods

2.1. Mercury Species Analysis

Different extraction methods for extracting MMHg, adapted from previous studies, were tested. The methodology used in this research for each extraction method are explained below.

2.1.1. Acid Extraction

The acid extraction method was adapted from Masbou et al. (2013). Deionized water was used for all method development and testing. Approximately 0.5 g of dry sediment was weighed into a 50 mL falcon tube. 5 mL of 30% w/w NaBr (Millipore Sigma) in 4 M H_2SO_4 (deionized grade 95%+, Fisher), 10 mL 2.5% w/w $CuSO_4$ (A.C.S reagent grade 98%, BDH), and 10 mL of toluene (A.C.S. reagent grade, Fisher) were added to the falcon tube. The sample was shaken on a horizontal shaker table at 200 rpm for 1h. During the extraction, the MMHg was freed from the sediment matrix and the extracted MMHg was converted to MMHgBr, which was transferred to the organic toluene phase. 8 mL of the toluene phase was transferred to a 15 mL falcon tube containing 4 mL of 0.005 M sodium thiosulphate (reagent grade 99%+, Caledon). The falcon tube was manually shaken for 1 min to convert the MMHgBr to a stable MMHg-thiosulphate, complex which was back extracted into the aqueous phase. The aqueous phase was collected and stored at 4 °C until analysis.

2.1.2. Alkaline Extraction

The alkaline extraction method was adapted from Tang et al. (2023). Approximately 0.2 g of sediment was added to a 15 mL falcon tube. 2 mL of 25% KOH (A.C.S. reagent grade 85%+, Sigma Aldrich) in methanol (A.C.S. reagent grade, Fisher)

was added to the tube. The tube was thoroughly manually shaken, then placed in a shaker (200 rpm) at 70°C for 4 h. The sample was diluted to 10 mL with deionized water and was left undisturbed for at least 4 h to let the solid particles settle to the bottom of the tube. The samples were stored at 4 °C until analysis.

2.1.3. Distillation

The distillation extraction method is adapted from EPA Method 1630 (1998). Approximately 0.5 g of dried sediment was added to a 30 mL Teflon vial. To the vial, 0.5 mL of 9 M H_2SO_4 (reagent grade 95%+, Fisher), 200 µL 20% KCl (A.C.S. reagent grade 99%+, Sigma Aldrich) and 10 mL deionized water were added. The H_2SO_4 was added to liberate the MMHg from the organic and inorganic sites present in the sediment, and the KCl to promote the formation of MMHgCl, which was the form that was co-distilled with water vapour (Perez et al., 2017). Distillation tubes were connected from sample vials to receiving vials containing 5 mL of deionized water. During the distillation, the vials were purged with nitrogen gas on a custom aluminum heating block at 125°C, until ~85% of the original volume was distilled. Distillations took approximately 1.5 h.

A modified distillation method was also tested using larger volumes of sediment (0.5 – 5 g) in 60 mL Teflon vials. 1 mL of 9 M H_2SO_4, 400 µL 20% KCl and 20 mL deionized water were added. 60 mL receiving vials were used, containing 5 mL of deionized water. Again, the distillation was stopped when ~85% of the volume had been distilled, which took ~2.5 h. Samples were stored at 4° C until analysis.

2.1.4. Solid Phase Extraction

Based on research by Chen et al. (2010) and Rosera et al. (2020) an anion exchange resin was tested as a method to remove inorganic mercury from an extracted solution. The resin used was AG® 1-X4 (200-400 mesh, chloride form, Rio-Rad). Samples were acidified to a final concentration of 0.1 M HCl (trace metal grade, Fisher). This provided a source of chloride ions to form neutral MMHgCl and anionic chloride complexes with inorganic mercury ($HgCl_3^-$ and $HgCl_4^{2-}$). The resin was prepared by first washing with deionized water and removing the finer grains of resin that floated. 1 mL of the resin was added to a borosilicate chromatography column. The column was prepared in sequence with 20 mL 0.05% L-cysteine (Sigma Aldrich) in 4 M HNO_3 (trace metal grade, Fisher), 20 mL 4 M HNO_3, 20 mL of deionized water and 10 mL of 0.1 M HCl. The sample was pumped through the column at a rate of ~3 mL/min. The sample was then passed through the column; the neutral MMHgCl was passed unretained through the column and the anionic mercury-chloride complexes were retained on the column. The eluate from the column was collected in a receiving vial as well as any additional elution volume of 0.1 M HCl and stored at 4 °C until analysis.

2.1.5. MMHg and THg Concentration Analysis

To assess the efficiency of extraction methods, measurement of the THg and MMHg concentrations were required. THg concentration was measured using the Tekran® 2600, and MMHg concentrations were measured using the Tekran® 2700. Concentrations were calculated using external calibration by comparing instrument response from samples to a calibration curve made from either a stock mercury standard (SPEX CertiPrep) or a stock MMHg standard (Thermo Scientific), measured at the

beginning of every analysis session. For THg, analysis samples were added to a glass vial and diluted, if required, for a final volume of 25 mL. 60 µL of 20% $SnCl_2$ (reagent grade 98%, Sigma-Aldrich) in 10% HCl was added to the samples and a Teflon septa cap was places on the vial. For MMHg analysis, the sample was transferred to a glass vial, 225 µL of acetate buffer (made from sodium acetate (A.C.S. grade, Fisher) and glacial acetic acid (A.C.S. grade, Fisher)) was added to adjust the pH to 4.9. Then, 30 µL tetraethylborate (Sigma Aldrich) was added to the vial. The tetraethylborate reacts with the mercury species in the sample, forming volatilize ethylmercury species, which are purged from the solution for analysis. Alkaline digestions were pH-adjusted using a citrate buffer made from citric acid (A.C.S. grade, BDH), and sodium citrate tribasic dihydrate (reagent grade, West Lab).

2.2. Isotope Ratio Analysis of Mercury

THg isotope ratios were measured using a cold vapour system for sample introduction to the MC-ICP-MS. The methodology for sample preparation, and analysis using the MC-ICP-MS is detailed below.

2.2.1. Preparation of Solutions and Standards

All samples prepared for isotope ratio analysis were prepared using deionized water. A 1 ng/mL Hg solution of NIST 3133 in 10% HCl was prepared as the bracketing standard for all isotope ratio measurements. In the same fashion, a solution of NIST 3177 (Almaden) was also prepared to act as a secondary calibration standard to ensure the instrument was measuring correct delta values. A 10% HCl solution was prepared to rinse the CV system between samples. For mass bias correction, a Tl solution of 10 ng/mL

NIST 977 was prepared in 2% HNO_3 and a 2% HNO_3 solution was prepared to rinse the Aridus. The final solution prepared for analysis was a 3% $SnCl_2$ solution in 10% HCl.

2.2.2. Sample Digestion for Mercury Isotope Ratio Analysis

To extract mercury from sediment samples for isotope ratio analysis, samples were digested using an acid digestion. 0.5 – 1.5 g of sediment was weighed into a glass vial and digested on a hot plate at ~110°C using a mixture of nitric/sulphuric acid (7:3 v/v). Digests were left on the hot plate overnight and then diluted to 25 mL with deionized water and stored in a dark place at room temperature until analysis. After digestion, samples were analysed on Tekran® 2600 to assess THg concentration, and samples were diluted prior to analysis to a concentration of 1 ng/mL to match the concentration of the NIST 3133 standard.

2.2.3. Measurements of Mercury Isotope Ratios

The instrument set up for measurement of mercury isotope ratios is illustrated in **Figure 2.1**. Briefly, the sample was pumped into the custom CV system at ~1.5 mL per minute. The sample was mixed with $SnCl_2$ using a Teflon t-connector in the tubing prior to entering the CV system. The Tl vapour was created by the Aridus desolvation system and introduced at the top of the CV system. A mix gas flowed through the bottom of the CV system to sweep the reduced Hg(0) out of solution and into the plasma of the MC-ICP-MS (Nu Plasma II).

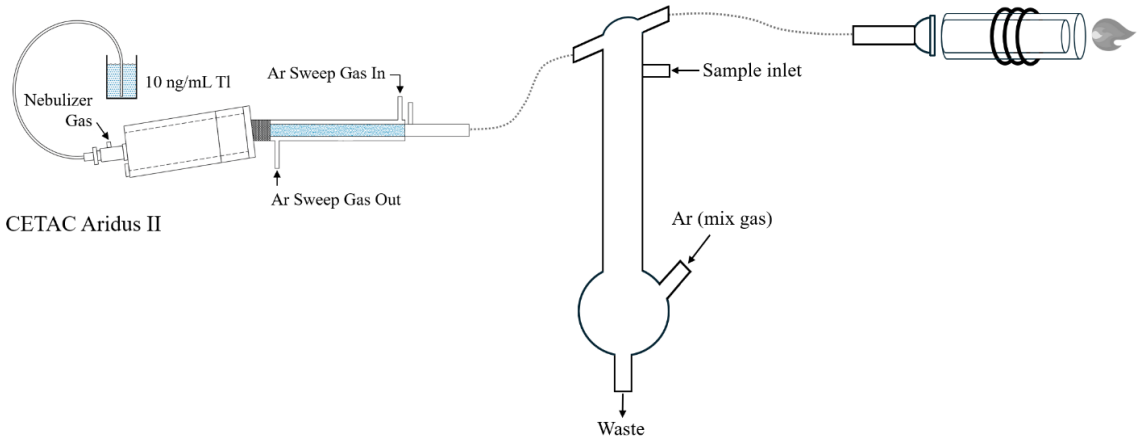

Figure 2.1. Schematic of setup of the MC-ICP-MS used for the measurement of mercury isotope ratios.

The instrument set up required three gases. The mix gas at the bottom of the CV, the nebulizer gas, which was connected to the Aridus to nebulize the Tl solution, and the sweep gas is added to remove water vapours that permeate the porous membrane in the Aridus. The typical settings for the gases and for the Faraday cup set up are displayed in **Table 2.1** and were optimized at each measurement session to achieve maximum response. The other parameters, such as torch position, high voltage, quads, source voltage and transfer voltage, were also adjusted daily to optimize sensitivity. All samples were diluted to 1 ng/mL and during every analytical session, the NIST 3177 standard was measured every 5 – 8 samples to ensure correct delta values were being measured. The method file used for analysis consisted of 2 blocks of 30 measurements each, with an integration time of 1 sec. Ratios that deviated more than 2 SD from the average were removed automatically by the Nu Plasma software.

Table 2.1. MC-ICP-MS operating parameters.

Parameter	**Setting**							
Mix Gas	0.03-0.05 L/min							
Neb Gas	30.0 psi							
Sweep Gas	3.2-3.6 L/min							
Faraday Cup Configuration	H4	H3	H2	H1	Ax	L1	L2	L3
	^{205}Tl	^{204}Hg	^{203}Tl	^{202}Hg	^{201}Hg	^{200}Hg	^{199}Hg	^{198}Hg

2.3. Compound Specific Isotope Ratio Analysis

The compound specific measurement of MMHg isotope ratios was accomplished by coupling the Tekran® 2700 to the MC-ICP-MS. The methodology for measuring MMHg isotope ratios, as well as the different approached for calculating isotope ratios from the raw data are detailed below.

2.3.1. Coupling GC to MC-ICP-MS

The GC used in this research was the Tekran® 2700. The typical automated sample analysis involved first the purging of the ethylated mercury species from solution using argon gas onto a Tenax® trap. At the end of the purge, the Tenax® trap oven was preheated to 170°C and argon gas was passed through the trap to desorb the mercury species off the trap and onto the GC column. During the desorption, the temperature of the trap oven continued to rise. Mercury species were separated by the GC and eluted in the following order: elemental mercury, methyl-ethyl mercury (represents the MMHg in sample), di-ethyl mercury (represents Hg(II) in sample). Once the mercury species exited the GC, they passed through the pyrolizer where they were thermally decomposed into elemental mercury, which was moved into a quartz cuvette to be detected by Cold Vapor

Atomic Fluorescence Spectrophotometry (CVAFS). The sample gas was then carried out of the Tekran via the cell vent and mercury species were directed to the MC-ICP-MS. The run time for one sample through the Tekran® 2700 was 660 sec or 11 minutes.

The instrument set up of the GC coupled with the MC-ICP-MS is displayed in **Figure 2.2.** The set up was very similar to the set up for THg isotope ratios, with the addition of the GC cell vent line added using a glass t-connector right before the torch. This set up allowed the analysis of calibration standards (NIST 3133 and NIST 3177) using the CV system to ensure MC-ICP-MS tuning resulted in correct isotope ratios before sample analysis using GC. When analysing samples using GC, DI water was run through the CV system. Since all the mercury species were pyrolyzed in the Tekran®, the mercury entering the MC-ICP-MS was always in the form Hg(0), same as when using the CV system alone.

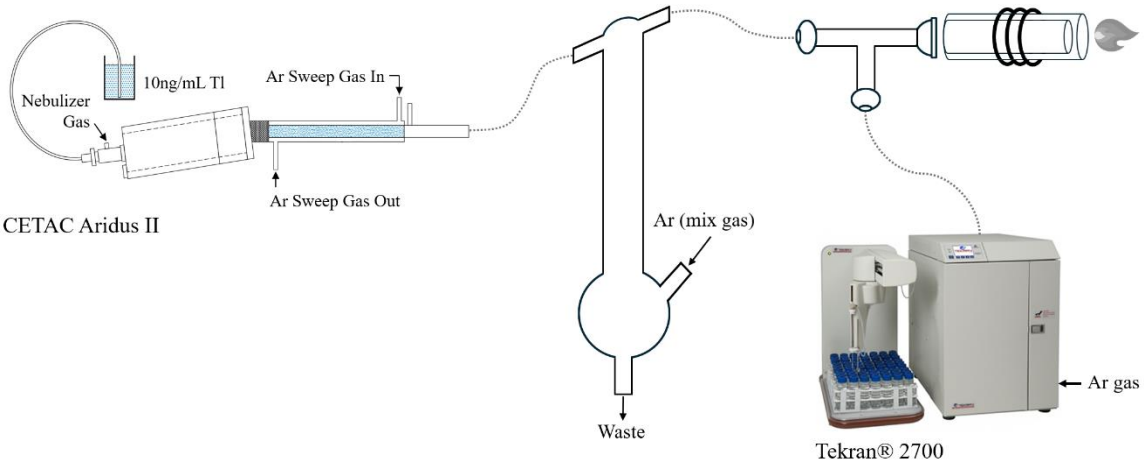

Figure 2.2. Schematic setup of the GC coupled to MC-ICP-MS used for the measurement of MMHg isotope ratios.

All data measured using the Tekran® was measured using the Time Resolved Analysis (TRA) utility in the Nu Plasma software for measuring transient signals. In TRA

mode, the signal intensities were measured for the duration of the data acquisition. The TRA mode permits the use of a trigger, which allowed an external instrument to trigger the MC-ICP-MS to start and stop data acquisition. The Tekran® was electronically connected to the MC-ICP-MS and the trigger was used to start data acquisition on the MC-ICP-MS at the beginning of the detection by CVAFS (at 360 sec) and end the data acquisition at the end of the Tekran® run (at 660 seconds).

The MC-ICP-MS tuning used with the GC coupling was very similar to the tuning for THg isotope ratio analysis. The gas and Faraday cup set up were the same as **Table 2.1.** Tuning of all other parameters was also completed daily to maximum response. The integration time used for most measurements was 0.5 sec, but 1 sec was also tested.

2.3.2. Data Processing

The application IsoCor created by Tukhmetova et al. (2022) was used to calculate the isotope ratios from the transient peaks. To use this application, the raw data from the MC-ICP-MS was exported. The raw data files of the sample and the NIST 3133 bracketing standards were combined and saved as .TXT files in order to be imported to IcoCor. The mass bias factor had to be calculated manually for each peak and the average mass bias factor calculated throughout the duration of the peak was used.

IsoCor includes four different baseline estimation methods, SNIP, TopHat, ConvexHull and median that are used for baseline correction and detection of the boundaries of the peaks. The methods are used to estimate a dynamic baseline, which is then subtracted from the intensities during the peaks for baseline correction during isotope ratio calculation. The SNIP method uses and algorithm that identifies regions in

the chromatogram that are baseline rather than peaks. The chromatogram signal is split into many overlapping windows and the algorithms identifies low points in each window that could be baseline. As the algorithm moves to more windows, the estimated baseline is updated. The TopHat method is a very straightforward algorithm that estimates the baseline by smoothing the data to reduce the noise. The ConvexHull method estimates the baseline by creating a boundary that wraps around the data points. This boundary is known as the convex hull and represents the estimated baseline. Finally, the moving median method estimates the baseline by determining the median value within a window of a default number of data points. The window is moved by one data point all the way along the signal. The median values result in the estimated baseline. The SNIP method is ideal for signals with very noisy backgrounds, the ConvexHull and TopHat are useful when the baseline changes throughout the signal, and the median method is a very simple method that is useful when the peaks are well defined.

All isotope ratios measured in this work are reported with their associated external precision, reported as 2 standard deviations (2 SD). The application calculates isotope ratios using three different methods, point-by-point (PBP), peak area integration (PAI), and linear regression slope (LRS), using different percentages of the peak. The first measurements of mercury isotope ratios from transient signals included a fourth option for calculating isotope ratios called the peak apex method. In this method, the isotope ratio is calculated from the highest signal intensity point. The rational is that statistically the most accurate ratios should occur at the highest count rate (highest signal intensity), however this method was proven to be quite inaccurate as the isotope ratio is calculated using only one data point (Dzurko et al., 2009). An illustration of the different calculation

methods is given in **Figure 2.3.** These methods were described briefly in chapter one but will be discussed in detail below.

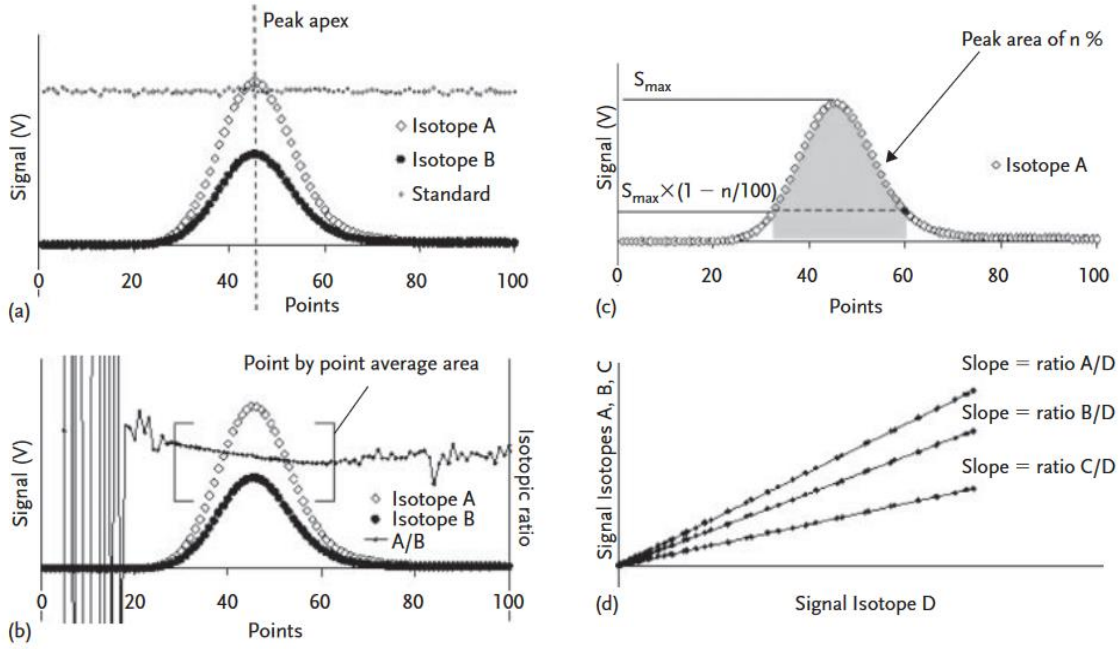

Figure 2.3. Illustration of different methods for calculating isotope ratios from transient signals: a) peak apex b) point-by-point c) peak area d) linear regression slope. From Epov et al., 2012.

The PBP method is also called the average peak ratio method. In this method, a certain percentage of the peak is chosen and the isotope ratio for every integration time point is calculated. Previous studies have averaged the isotope ratios over the duration of the peak. IsoCor however, uses the median isotope ratio of all integration time points, as it is more robust towards outliers that occur at the shoulders of the peak.

Using the PAI method, the isotope ratio is calculated by dividing the integrated peak area of two isotopes. Again, different percentages of the peak can be selected. The accuracy of this method is generally dictated by the choice of area for integration. The

start and stop times for integration is generally determined from the ^{202}Hg peak and applied to the peaks for the other isotopes.

The final method of LRS requires no baseline subtraction. In this method, the isotope ratio is given as the slope of a linear regression line between the plotted intensities of two isotopes as a function of one another. All points from the peak are used including the baseline hence no additional background correction is required (Dzurko et al., 2009; Epov et al., 2012). This method has proven to give quite accurate and precise ratios by multiple authors (Bouchet et al., 2018; Epov et al., 2010; Queipo-Abad et al., 2019).

2.4. Field Sampling

Field samples for this research were collected in Kangiqsualujjuaq, Quebec. Kangiqsualujjuaq is a fly-in, Inuit community located in the Nunavik region in northern Quebec and is one of fourteen communities in Nunavik. The community is located at the mouth of the George River on the east coast of Ungava Bay (**Figure 2.4**). Kangiqsualujjuaq is located in a zone of discontinuous permafrost, meaning that although between 50 – 90% of the ground is at or below 0°C year-round, there are areas that are permafrost-free (Heginbottom, 2002).

Figure 2.4. Location of Kangiqsualujjuaq, Quebec.

Sediment samples were collected in both the winter and the summer. Sampling occurred in March 2023 and September 2023. Two thermokarst lakes were chosen for sampling in both seasons: Lake 5 (58°45'26.0"N, 66°00'33.4"W) and Lake 11 (58°45'30.9"N, 66°00'51.5"W), a third lake was sampled only in the summer: Lake 9 (58°45'31.0"N, 66°00'52.9"W) (**Figure 2.5**). The lakes were chosen primarily for their size as there was concern that the smaller lakes would be completely frozen during the winter, not allowing for water sampling, which other researchers were collecting. **Table 2.2** displays the depth and ice cover (winter) for each Lake 5 and Lake 11 at the location of sampling. In the winter, the lakes were covered in 30 – 50 cm of snow but in the summer different types of vegetation surrounding the lakes could be seen (**Figure 2.6**).

Figure 2.5. Location of thermokarst lakes.

Table 2.2. Lake and ice depth of both lakes (Lake 9 not measured). Lake depth in winter measured from ice surface to bottom of lake.

Season	Parameter	Lake 5	Lake 11
Winter	Lake depth (m)	0.8	2.35
	Ice Depth (m)	0.5	0.85
Summer	Lake depth (m)	1	0.75

Figure 2.6. Lake 5 (left), Lake 11 (right) in September 2023.

Before any samples were collected, the physiochemical properties of the lakes were measured using a Hydrolab DS5 multi-probe sensor (OTT Hydromet). Relevant parameters include measured include temperature, pressure, dissolved oxygen (DO), total dissolved solids (TDS), and pH (**Table 2.3**). These lakes were typical for thermokarst lakes, exhibiting high concentrations of dissolved organic carbon as indicated by high TDS values and anerobic conditions, specifically in the winter, as indicated by low dissolved oxygen.

Table 2.3. Physiochemical properties of lakes in summer and winter.

Lake 5 - Winter

Depth (m)	Temp (°C)	Pressure (kPa)	DO (%)	DO (mg/L)	TDS (mg/L)	pH
0.00	0.490	101.88	17.3	2.36	177.5	7.11
0.25	0.231	101.89	9.7	1.38	177.6	7.00
0.50	0.364	101.90	6.6	0.83	176.4	6.90
0.75	0.260	101.90	4.1	0.69	176.3	6.86
0.80	0.230	101.89	2.7	0.38	176.8	6.79

Lake 5 – Summer

Depth (m)	Temp (°C)	Pressure (kPa)	DO (%)	DO (mg/L)	TDS (mg/L)	pH
0.00	7.160	101.94	90.5	10.91	26.111	6.22
0.25	7.053	101.94	87.9	10.66	28.621	6.09
0.50	6.937	101.94	87.3	10.62	32.662	6.08
0.75	6.629	101.94	86.1	10.55	31.613	6.05
1.00	6.461	101.93	85.8	10.57	29.404	6.01

Lake 11 – Winter

Depth (m)	Temp (°C)	Pressure (kPa)	DO (%)	DO (mg/L)	TDS (mg/L)	pH
0.00	0.190	99.73	43.4	6.13	2.519	7.30
0.25	0.446	99.73	8.8	1.21	173.171	7.27
0.50	0.418	99.71	3.8	0.54	173.3	7.24
0.75	0.355	99.73	1.8	0.26	172.91	7.22
1.00	0.264	99.74	1.1	0.15	172.81	7.20
1.25	0.350	99.73	0.6	0.09	171.61	7.18
1.50	0.527	99.72	0.2	0.03	170.07	7.17
1.75	0.952	99.72	–0.1	–0.01	171.11	7.16
2.00	0.982	99.73	–0.2	–0.02	172.59	7.14
2.25	1.029	99.72	–0.2	–0.03	173.66	7.12

Lake 11 – Summer

Depth (m)	Temp (°C)	Pressure (kPa)	DO (%)	DO (mg/L)	TDS (mg/L)	pH
0.00	7.318	101.07	84.7	10.17	119.387	6.94
0.25	7.238	101.07	82.1	9.91	111.3234	6.82
0.50	6.742	101.07	82.1	10.09	107.765	6.80
0.75	5.976	101.06	81.1	10.09	106.66	6.82

The sediment samples were collected using a corer. One core sample of approximately 20 – 30 cm in length was taken from each lake. After collection, the samples were kept in the corer tube and transported back to the research station for processing. In the laboratory, each core was extracted, thoroughly homogenized and split into five PTFE (polytetrafluoroethylene) bottles. Two amendments were used to promote mercury methylation. Sulphate was added because it is known to increase methylation (Jeremiason et al., 2006), and lactate was used as it is a source of carbon and an electron donor in the biological sulphate reducing process (Oyekola et al., 2009). Amendments were added to the bottles according to **Table 2.4**. One sample received no amendments and was immediately placed in the freezer to stop bacterial activity. After adding the amendments, samples were incubated for 12 h at room temperature before being placed in the freezer. Samples were shipped frozen to Trent University. They were then defrosted and dried at 60°C for at least 48h or until their weight no longer changed. The samples were then homogenized using a mortar and pestle and stored in airtight containers until analysis.

Table 2.4. Amendments added to subsamples from each lake.

Sample	Amendment	Incubation Time (h)
L5/9/11 NA T0	–	0
L5/9/11 NA T12	–	12
L5/9/11 L	5 mM Lactate	12
L5/9/11 S	5 mM Sulphate	12
L5/9/11 L+S	5 mM Lactate and 5 mM Sulphate	12

2.5. Quality Assurance and Control

Throughout method development, blanks were always prepared and measured to ensure no contamination occurred during the protocol. For distillation, the blanks had an average MMHg concentration per distillate of 6 ± 10 pg (n=14). Reference material was used when testing extraction methods to determine recovery. The certified reference estuarine sediments BCR 580 and IEAE 475 were used along with two in-house reference materials.

During the digestion of sediment for THg isotope analysis, IEAE 475 was also digested to assess recovery of the method. The average recovery was 108±8%. Digestion blanks had an average THg concentration of 17 ± 9 pg (n=5) in the total digestion sample. The overall average and uncertainty value for NIST 3177 isotope ratio determinations was δ^{202}Hg = – 0.54 ± 0.1‰, Δ^{199}Hg = – 0.00 ± 0.01‰ (n=21, 2 SD), which is consistent with the certified values of δ^{202}Hg = – 0.56 ± 0.03‰, Δ^{199}Hg = – 0.03 ± 0.02‰. There currently exists no certified sediment reference materials for mercury isotope ratios. However, the THg isotope ratios for BCR 580 have been reported by a few authors in literature and were measured in this work to compare to published values. The overall average and uncertainty values for BCR 580 was δ^{202}Hg = – 0.44 ± 0.06‰, Δ^{199}Hg = – 0.04 ± 0.04‰ (n=4, 2 SD), which is consistent with previously reported values (**Table 2.5**) (J. Liu et al., 2011; Reinfelder & Janssen, 2019; Yin et al., 2015; Zhou et al., 2024).

Table 2.5. THg isotopes composition of BCR 580.

Reference	$\delta^{202/198}$	2SD	Δ^{199}	2SD
Liu et al. (2011)	–0.46	0.04	–0.02	0.01
Janssen et al. (2015)	–0.48	0.06	–0.01	–
Yin et al. (2015)	–0.44	0.08	–0.03	0.04
Reinfelder et al. (2019)	–0.45	0.05	–0.01	0.00
Zhou et al. (2024)	–0.49	0.10	–0.05	0.00
This Work	–0.44	0.06	–0.04	0.05

2.6. Statistical Analysis

Statistical analysis of differences in isotope ratio values between various samples were conducted using Microsoft Excel. T-tests were used to determine if results were statistically different. Differences between samples were considered significant for $p < 0.05$.

Chapter 3: Results and Discussion

3.1. Acid Extraction

The acid extraction method was initially tested following the method detailed in section 2.1.1. This method has two modifications from the method described by Masbou et al. (2013). They transferred 3 – 6 mL of the toluene extract to the new falcon tube for back extraction and diluted the final sodium thiosulphate phase five times prior to concentration analysis. This work used 8 mL of the toluene extract and did not dilute the final sodium thiosulphate phase, to increase the amount of MMHg in the final solution for analysis. The dilution and lower transfer of toluene restricts the method to samples with very high concentrations of MMHg, limiting its versatility.

Initially, this method was tested on a pure MMHg standard. 12 ng of the MMHg standard was added to the falcon tube with the extraction reagents. A 250 µL aliquot of the sodium thiosulphate phase was analysed using the Tekran® 2700. The measured concentration of MMHg added to the extraction solution was 0.49 ng, meaning the percent recovery was only 4% (**Table 3.1**). Thiosulphate is known to have high complexing affinity for organic mercury, which could be interfering with the ethylation of MMHg required for MMHg to be volatilized and therefore detected. To test if there was interference with the ethylation, a 12 ng spike of MMHg was added to 4 mL of sodium thiosulphate, and again a 250 µL aliquot was analysed. The recovery was again very low, only 7% (**Table 3.1**), suggesting that there was interference with the ethylation. Avramescu et al. (2010) tested different concentrations of thiosulphate for extraction and different volumes of the thiosulphate solution for analysis and found that high recoveries (+100%) were achieved using a thiosulphate concentration of 0.1 mM and 0.5 mL of

thiosulphate for analysis. This would correspond to 0.05 mmol thiosulphate in the solution to be analysed. In comparison, the solutions analysed in this work contained 1.25 mmol thiosulphate. Although additional dilution would improve the MMHg recovery and suffer from less interference with ethylation, this would lead to solutions with even lower concentrations of MMHg. The average concentration of mercury in sediment from uncontaminated areas range from 30 ng/g to 100 ng/g (Gworek et al., 2020). With only 1% of the mercury being methylated, the amount of MMHg extracted from one gram of sediment would range from 0.3 – 1 ng, which with additional dilution is not sufficient for isotope ratio measurement.

Table 3.1. Average measured mass of MMHg and recovery of MMHg from acid extraction tested with spike additions of MMHg and from MMHg added to sodium thiosulphate.

Sample	n	Expected Mass of MMHg (ng)	Average Measured Mass of MMHg (ng)	Recovery (%)
MMHg Spiked Extraction Solution	3	12	0.49	4.12
MMHg Spiked Thiosulphate	3	12	0.86	7.13

The back extraction into thiosulphate in this method is used to selectively separate MMHg from the other forms of mercury. To avoid using thiosulphate, a modified method was tested using NaBr and $CuSO_4$ to extract mercury species for the sediment matrix, and then isolating the MMHg using solid phase extraction.

3.2. Solid Phase Extraction for Separation of MMHg

Initially, the retention of inorganic mercury by the AG® 1-X4 resin was tested. A solution of 15 mL of 5 ng/mL inorganic mercury was passed through the resin. The

sample and rinsing after leaving the column had very low levels of inorganic mercury, corresponding to a concentration of less than 4 pg/mL. A solution of 0.05% L-cysteine in 0.5 M HNO_3 was used to elute the mercury from the resin as used by Chen et al. (2010). The average recovery was 99 ± 5% (**Table S - 1**). These results indicate that the resin readily retains inorganic mercury which is fully eluted by L-cysteine is in agreement with the findings of Chen et al. (2010).

Although MMHg is not retained on the resin, once passing a sample through the resin an additional volume of eluent was required to fully remove all the MMHg from the column. In order to dilute the sample as little as possible, the ideal elution volume is the smallest volume that still achieves full recovery of the MMHg. Elusion volumes from 0 to 35 mL were tested. Elusion volumes of 10 mL and above had recoveries over 100% (**Figure 3.1**), and therefore 10 mL was concluded to be the ideal elution volume.

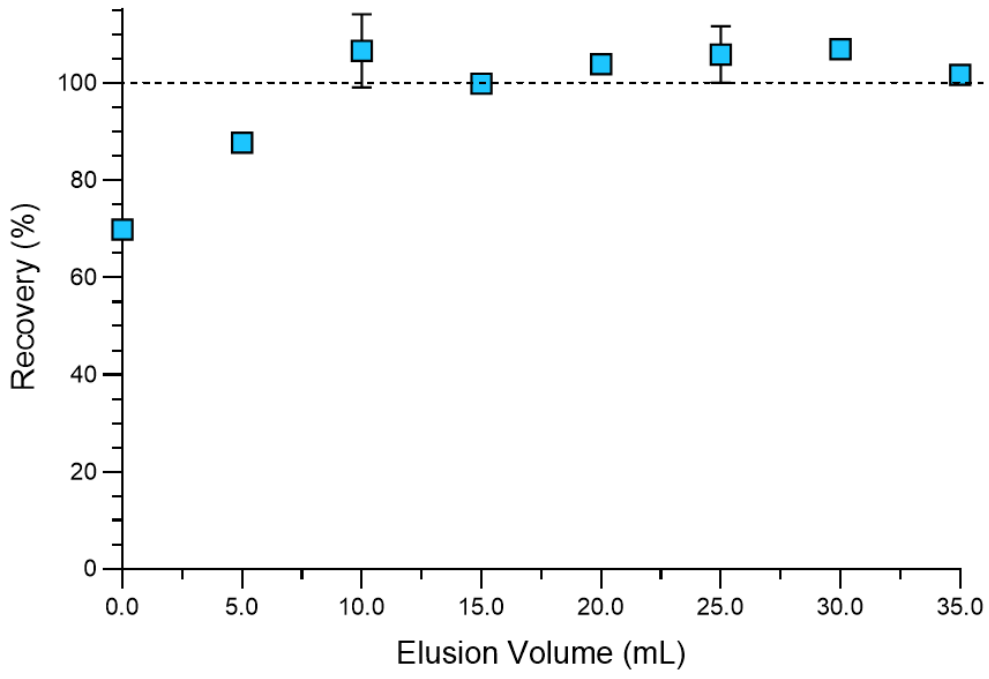

Figure 3.1. Recovery of MMHg from resin with different elusion volumes.

To ensure that the resin did not cause fractionation of MMHg, stock MMHg was passed though the resin and analysed by MC-ICP-MS. The samples were first oxidized by adding 0.25 mL BrCl to degrade the MMHg. Just before analysis, 0.1 mL of 20% aqueous hydrochloride hydroxylamine solution was added to the samples to neutralize the excess BrCl. Because there is no stock MMHg solution with certified isotope ratios, the stock MMHg (Sigma Aldrich) was measured after decomposition with BrCl multiple times to compare to the resin samples (**Table 3.2**). The isotopic compositions of the samples passed through the resin were not statistically different than the MMHg standard analysed directly ($p > 0.05$, unpaired t-test).

Table 3.2. Isotopic composition of stock MMHg and MMHg passed through resin.

Sample	n	δ^{202}	2SD	Δ^{199}	2SD	Δ^{200}	2SD	Δ^{201}	2SD
Stock MMHg	9	–1.15	0.06	0.09	0.02	0.04	0.04	0.04	0.03
Resin	4	–1.16	0.04	0.07	0.09	0.05	0.05	0.06	0.08

3.3. Isolation of MMHg from Acid Extraction

The modified acid extraction method was tested with a MMHg standard solution. To a falcon tube containing 5 mL of 30% w/w NaBr in 4 M H_2SO_4 and 10 mL 2.5% w/w $CuSO_4$, 12 ng of MMHg was added. After 1 h in the shaker, the sample pH was adjusted using KOH to a pH of 1. NaCl was added to the solution to provide a source of Cl^- to complex with MMHg to form neutral MMHgCl and the sample was passed through the resin. The recovery of MMHg through the resin was only 7% (**Table 3.3**). To determine if MMHg was not making it through the resin or if the MMHg was in the sample but was just not detected, the reagents were test independently. For isotope ratio measurement, to obtain the highest mass of MMHg, ideally the total extraction solution would be used.

Considering this, a 250 pg spike of MMHg was added to a vial with 5 mL of 30% NaBr in 4 M H_2SO_4, and a vial containing 10 mL 2.5% w/w $CuSO_4$. The acidic sodium bromide vial had to be neutralized using KOH due to it being so acidic, to bring the sample into a pH range of 4.9. The samples were analysed by the Tekran® 2700 and the recovery for the solution of NaBr and $CuSO_4$ were 1% and 12%, respectively (**Table 3.3**). This suggests that both reagents interfere with the ethylation of MMHg.

Table 3.3. Average measured mass of MMHg and recovery of MMHg of spiked acid digestion through resin, and of spiked samples of each reagent.

Sample	n	Expected Mass of MMHg (pg)	Average Measured Mass of MMHg (pg)	Recovery (%)
Spiked Acid Digestion through Resin	3	12000	850.0	7.1
Spiked NaBr	3	250	2.9	1.2
Spiked $CuSO_4$	3	250	29.5	11.8

MMHg forms a stable complex with bromide (Qian et al., 2000), which may be interfering with the ethylation. Pietilä et al. (2015) tested a solvent extraction method using KBr and $CuSO_4$. They found no interference from bromide for concentrations of 0.4 to 0.5 M. The concentration of NaBr in the vial tested in this study was 0.6 M, which may be too high causing the tetraethylborate is not able to complex with the MMHg in solution due to the stable formation of MMHgBr. Cu^{2+} has also been found to interfere with MMHg recoveries due to incomplete ethylation. Mansfield and Black (2015) found that concentrations as low as 0.01 mM decreased the MMHg recoveries, and concentrations of 10 mM resulted in only 35% MMHg recovery. The concentration of the samples tested in this study was six times higher than that at 60 mM, therefore the high

concentration of Cu^{2+} in solution is likely responsible for the poor MMHg recovery. Although dilution would likely eliminate the interference from these reagents, dilutions would lead to lower MMHg concentrations in the sample, which again is not ideal for isotope ratio measurements.

Although Cu^{2+} caused large interference with ethylation, Mansfield and Black (2015) did find that the addition of EDTA in excess of Cu^{2+} completely eliminated the interferences. Although this was not tried in this research, it could be an option to remove the interference from Cu^{2+}. It is also possible that a lower concentration of NaBr could be used and still have high recovery rates. The 30% NaBr solution correspond to a concentration of 2.9 M NaBr. Qian et al. (2000) used an extraction solution containing 0.38 M KBr and Pietilä et al. (2015) used 0.4 – 0.5 M KBr, both achieving high recovery of MMHg from samples. These lower concentrations should not cause the interference seen in this research.

Another alternative option would include the use of dichloromethane. Bloom et al. (1997) used a similar extraction method to this research using KBr, H_2SO_4 and $CuSO_4$. They then added 10 mL CH_2Cl_2 to transfer the MMHg into the organic phase. An aliquot of the organic phase was added to a purging vessel containing water, and the sample was purged with nitrogen to remove the CH_2Cl_2 leaving the MMHg in pure water matrix. This would result in a sample that would not contain either Cu^{2+} or Br^- which were the sources of interference with the current methodology, however each additional step does add additional possibilities of fractionation and creates a more time-consuming and labour-intensive method.

3.4. Alkaline Extraction

The alkaline extraction method was initially tested on the certified reference material BCR 580. This extraction method is not selective for MMHg. It liberates all forms of mercury present in the sediment into the extraction solution. Because sediment is only ~1% MMHg (Janssen et al., 2015), a large amount of inorganic mercury is also extracted. This means that when an aliquot of the extractant in analysed, a very large inorganic peak overshadows the small MMHg peak (**Figure 3.2**). The average measured concentration of MMHg in BCR 580 was 74 ± 2 µg/kg (n=3), which is quite similar to the certified concentration of 75 ± 4 µg/kg. The average recovery was 97 ± 3% (**Figure 3.3**), which is ideal as it means there should be no fractionation caused by the extraction method.

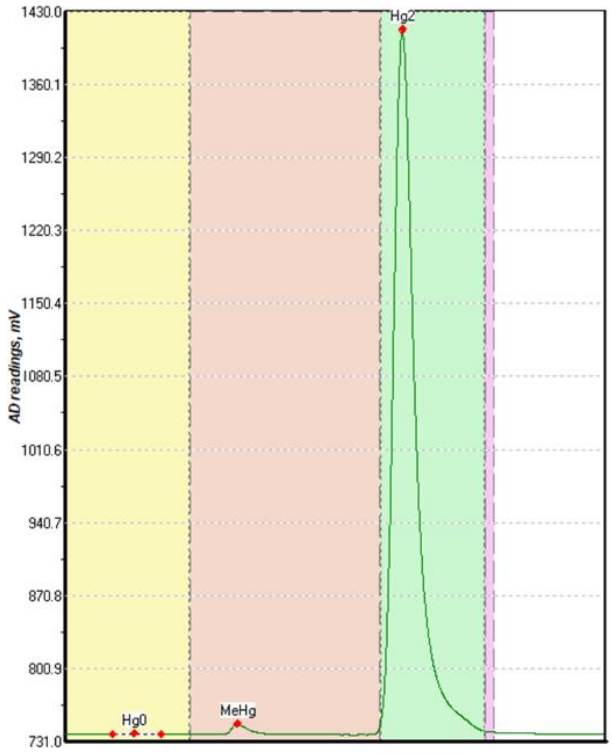

Figure 3.2. Chromatogram of alkaline extract analysed using Tekran 2700. Peak in yellow from Hg(0), peak in pink from MMHg, peak in green from Hg(II).

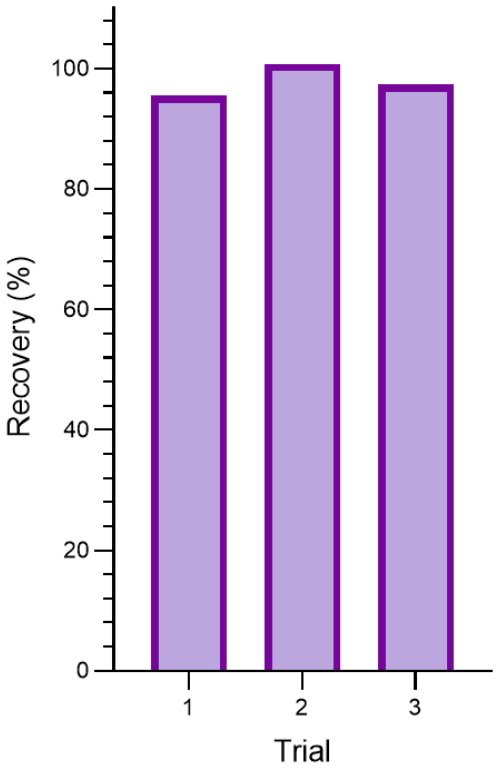

Figure 3.3. Recovery of MMHg for alkaline extraction method.

The large inorganic peak, however, is a concern for two reasons. First, the Tekran® 2700 in our experience does have some carryover between samples if the concentration in the previous sample is notably high. This is problematic because it could mean that there is carryover from the sample to the bracketing standard, affecting the calculated delta value. Second, this large inorganic peak could also be problematic in the MC-ICP-MS. Mercury is known to have significant memory effects (Harrington et al., 2004), and there is concern that the high inorganic signal would carryover into the MMHg peak of the following sample, or would lead to a continued rise in baseline signal, which would then interfere with the effectiveness of the baseline correction during isotope ratio calculation. To remove the inorganic mercury from the sample, solid phase extraction using the AG® 1-X4 resin was tested.

3.5. Isolation of MMHg from Alkaline Extraction

The use of the anion exchange resin for removing inorganic mercury from the solution was first tested using a MMHg standard solution. 50 ng of MMHg standard was added to the falcon tube containing the KOH in methanol solution. After the 4 h in the shaker and dilution to 10 mL, NaCl was added to the extractant solution to a concentration of 0.1 M to provide a source of chloride to complex with MMHg. The recovery of the alkaline solution with no pH adjustment though the resin was only 5.7 ± 0.7% (**Figure 3.4**). Then the resin recovery was tested again, this time by adjusting the pH of the alkaline extraction solution to a pH of 1 using HCl. This time the average recovery was 43.5 ± 1.6%. The exact reason for the loss of mercury in the eluate is unclear. However, during these experiments, the instability of MMHg in alkaline solutions was observed. The MMHg concentration in spiked solutions of the alkaline extract decreased by 25 – 40% in only 24 h. These observations are consistent with previous studies on MMHg stability. Ahmed & Stoeppler (1987) observed a 40% decrease in MMHg in just one day. They attributed the loss of MMHg to the formation of undetectable MMHg complexes. Either way, this instability and poor recovery makes the alkaline extraction a poor choice for extraction of MMHg for isotope ratio measurement.

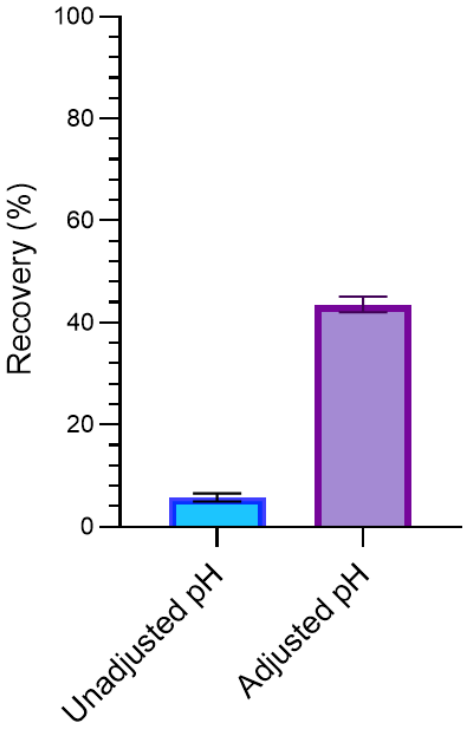

Figure 3.4. Recovery of MMHg in eluant after alkaline extraction and solid phase extraction.

3.6. Distillation

Distillation is a method for extracting MMHg from soil and sediment samples that is routinely used reliably by many studies with good recovery including Bloom et al. (1997), Horvat et al. (1993), Janssen et al. (2015), who all reported recoveries of between 80 – 100%. In this research, a recovery of 96 ± 10% (n=3) was achieved for BCR 580. The general methodology for distillation involves the use of 0.2 – 0.5 g of sediment. However, depending on the concentration of MMHg in the sediment, 0.5 g of sediment is likely not enough to extract sufficient MMHg for isotope ratio measurement. Therefore, the method was tested with increasing masses of sediment to determine if the method could be successfully scaled up to larger sample masses.

Instead of using costly certified reference materials, two in-house reference materials were used to evaluate distillation with larger sample masses. Although no certified values are available for these sediments, the MMHg concentration was determined by distilling many replicates (n=9) of 0.5 g of sediment (Ref Sed 1: 12.4 ± 1.4 ng/g, Ref Sed 2: 42.6 ± 2.0). Masses from 0.5 – 3 g of Ref Sed 1 were distilled and the MMHg concentration of the distillate was measured (**Figure 3.5**). From 0.5 – 2 g, the measured concentration of the distillates was within 15% of the previously determined average concentration. However, when 3 g of sediment was used, the measured concentration dropped by 30% meaning all the MMHg present in the sample was not being extracted. This is likely because of the decreasing water content of the resulting slurry, which lead to insufficient mixing between the reagents and the sediment. To alleviate this problem, a modified distillation method was tested which doubled the volumes of each of the reagents. The modified method also used larger 60 mL vials to provide more room for the sediment and reagents to mix. This modified method was very successful and was able to be scaled to 5 g of sediment and still fully extract all the MMHg from the sediment (**Figure 3.6**). Assuming an average THg concentration of 30 – 100 ng/g (Gworek et al., 2020), 5 g of sediment would extract approximately 1.5 – 5 ng of MMHg, which would be sufficient for isotope measurements.

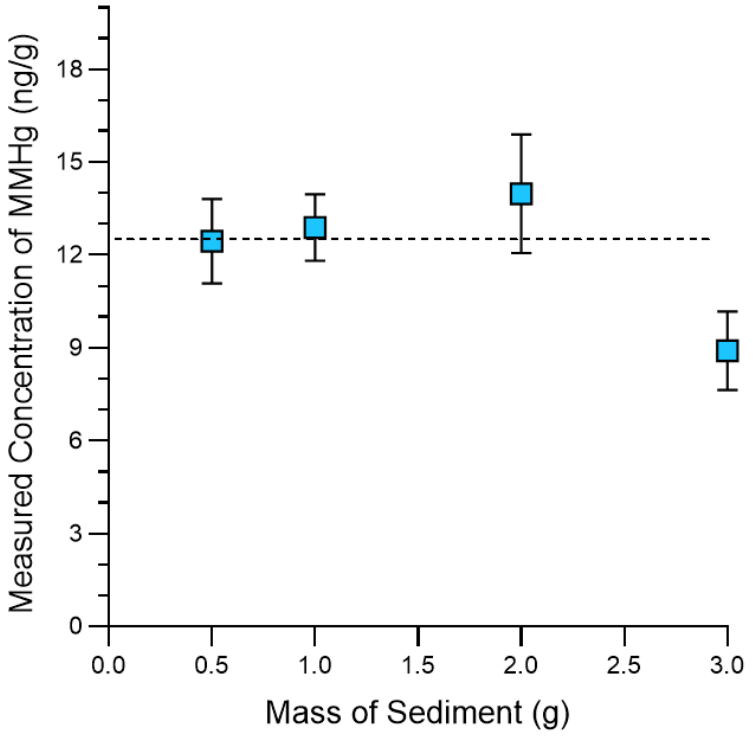

Figure 3.6. Measured MMHg concentration extracted by standard distillation method (10 mL slurry in 30 mL vials) using 0.5-3 g of sediment. Dashed line represents accepted sediment concentration.

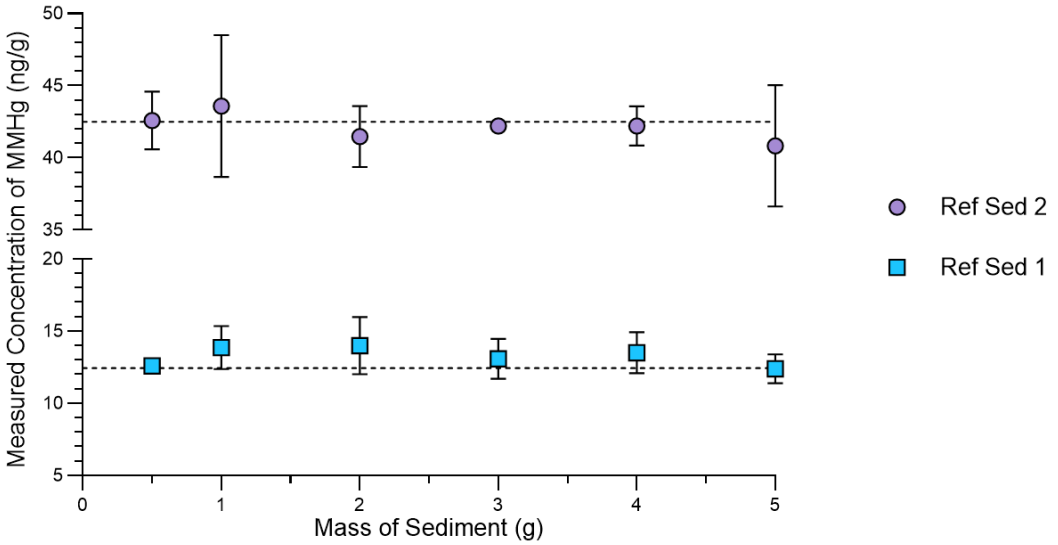

Figure 3.5. Measured MMHg concentration of two in-house reference sediments using the modified distillation method (20 mL slurry with 60 ml vials). Dashed line represents accepted sediment concentration.

During distillation, there is some inorganic mercury from the sample that is also carried over into the receiving vial, but to a much lesser extent than during alkaline extraction method. The peak area of the MMHg peak was 1 – 5 times larger than the inorganic peak (**Figure 3.7**). Since the different forms of mercury will be separated using GC prior to isotope ratio measurements, the small amount of inorganic mercury is not an issue.

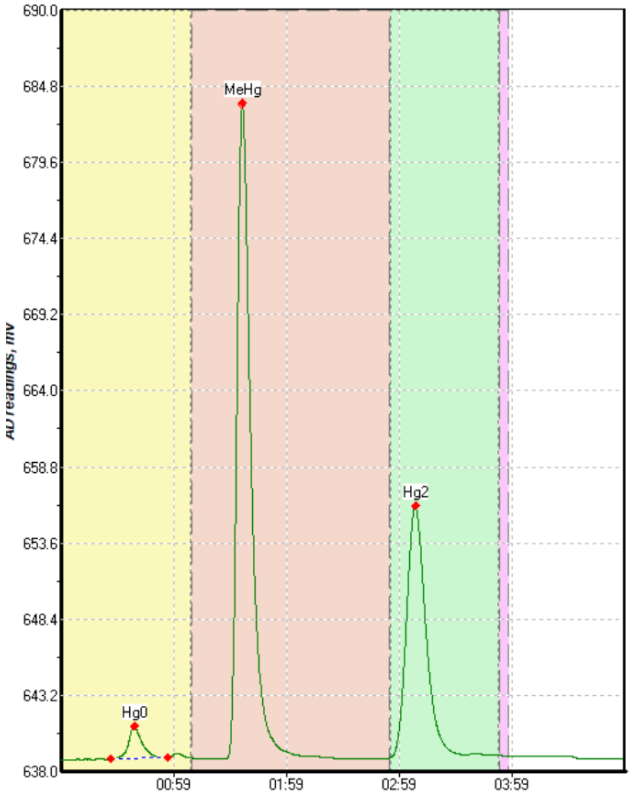

Figure 3.7. Example chromatogram from distillations. Although some inorganic mercury is present (green), peak height is much lower than MMHg (pink).

To test for Hg isotope fractionation, the stock MMHg was distilled and tested on the MC-ICP-MS. Spikes of 25 ng of the MMHg stock was added to 20 mL of deionized water and other reagents in the distillation vials. The samples were distilled to ~85% completion. Similar to the resin samples, the distillates were oxidized with BrCl and the

excess BrCl was neutralized with hydrochloride hydroxylamine before analysis. There was no statistical difference between the stock MMHg and the distilled samples ($p > 0.5$, unpaired t-test), and the recovery of the spike additions was 92 ± 5% (**Table 3.4**). As an additional check to ensure the isotope compositions of the MMHg as it was distilled were consistent, subsamples were taken four times during a distillation. These subsamples represented every 20% of the distillation, and the δ values for each fraction also showed no statistical difference with the stock MMHg (**Table 3.4**). 125 ng of MMHg was added to each distillation vial. The proportion of distilled of the MMHg however, is not equal across each 20% fraction. The mass of MMHg transferred to the receiving vial decreases as the distillation proceeds. This explains why recoveries of over 90% are possible when the distillations are stopped when only ~85% of the original volume is distilled.

Table 3.4. Isotopic compositions of distilled samples and the recovery of the added MMHg spike.

Sample	n	δ^{202}	2SD	Δ^{199}	2SD	Δ^{200}	2SD	Δ^{201}	2SD	% MMHg Recovery of Spike
Stock MMHg	9	–1.15	0.06	0.09	0.02	0.04	0.04	0.04	0.03	n/a
Full Distillation	4	–1.16	0.10	0.10	0.06	0.06	0.03	0.03	0.05	92
First 20% Fraction	3	–1.17	0.09	0.12	0.01	0.05	0.06	0.09	0.07	29
Second 20% Fraction	3	–1.20	0.05	0.09	0.04	0.02	0.05	0.05	0.07	26
Third 20% Fraction	3	–1.15	0.08	0.08	0.04	0.05	0.03	0.06	0.06	18
Fourth 20% Fraction	3	–1.18	0.11	0.11	0.03	0.08	0.10	0.03	0.05	11

The certified reference material BCR 464 (certified for Hg concentration) was also distilled and analysed. BCR 464 is a tuna fish sample, and although it is not certified for MMHg isotope ratios, values have been reported previously by a few authors. BCR

464 was analysed to ensure that the distillation of real sample material would also not cause isotope fractionation. This material was chosen because effectively all of the mercury present in the sample is MMHg. The certified total mercury concentration is 5.24 ± 0.10 mg/kg and the MMHg concentration is 5.50 ± 0.17 mg/kg. This allowed the distilled sample to be measured directly using the CV system on the MC-ICP-MS, with no GC separation required. The isotope ratios measured in this research were consistent with the values measured by other studies (**Table 3.5**).

Table 3.5. MMHg isotopic compositions of BCR 464.

Reference	δ^{202}	2SD	Δ^{199}	2SD	Δ^{200}	2SD	Δ^{201}	2SD
Bouchet et al. (2018)	0.70	0.11	2.32	0.06	0.08	0.06	1.96	0.12
Epov et al. (2008)	0.93	0.67	2.21	0.07	0.14	0.24	2.15	0.07
	0.65	0.30	2.52	0.44	0.05	0.46	2.11	0.46
Epov et al. (2010)	0.55	0.24	2.41	0.15	0.10	0.08	1.97	0.26
Masbou et al. (2013)	0.62	0.13	2.34	0.11	0.08	0.05	1.88	0.07
This work	0.70	0.09	2.28	0.11	0.13	0.08	1.87	0.08

Based on these results, distillation is an ideal extraction method, which is able to reliably extract MMHg from up to 5 g of sediment. It only extracts a small portion of inorganic mercury along-side the MMHg, which can be separated using GC. Most importantly, the extraction method imparts no fractionation on the extracted mercury. This is consistent with the findings of Dzurko et al. (2009), Janssen et al. (2015), and Rosera et al. (2020), who all found distillation caused no fractionation.

3.7. Isotope Ratio Analysis using GC

Using the TRA mode, the intensities of mercury isotopes were measured as mercury was eluted from the GC column. To import the data into IsoCor all data must be combined into a single file, containing the bracketing standards and the sample. An example of this is shown in **Figure 3.8** which displays the combined chromatograms of the NIST 3133 bracketing standards and the MMHg standard. The Tekran® provides baseline separation between the MMHg peak and the inorganic mercury peak. During the Tekran® run, MMHg is eluted at ~100 seconds and the peak width is ~40 seconds, and the inorganic mercury peak is eluted at ~200 seconds and has a peak width of ~25 seconds. ^{196}Hg was not measured because the low abundance would provide very low intensity and therefore an unstable signal.

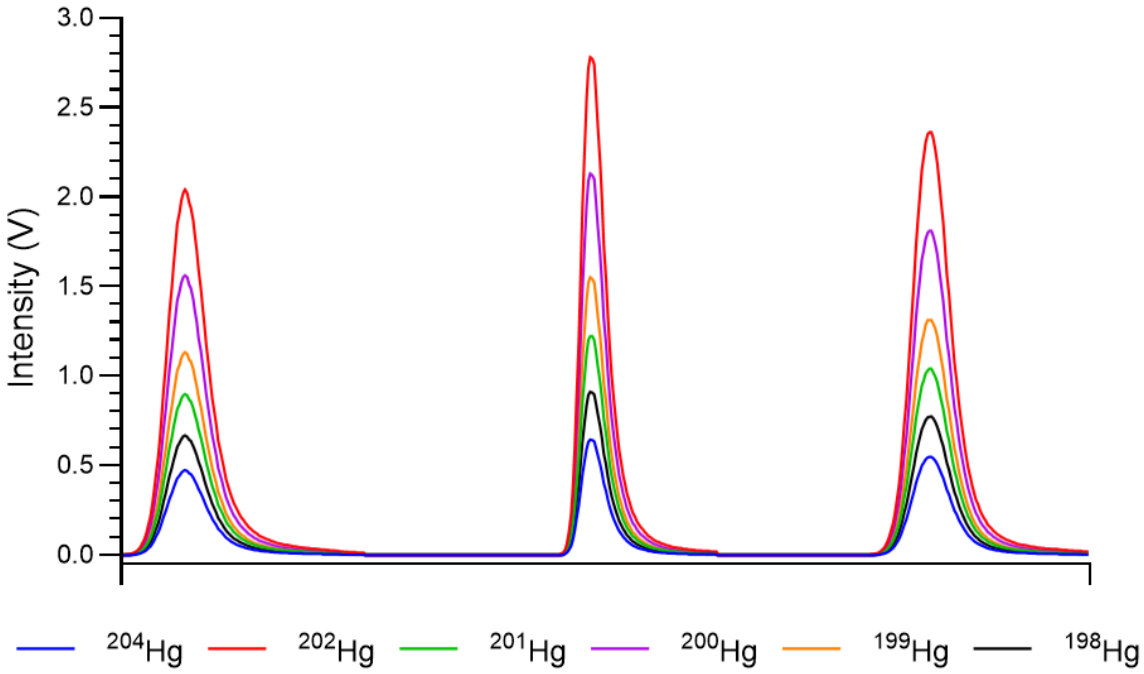

Figure 3.8. Combined chromatogram of bracketing standards and MMHg standard. Peaks 1 and 3 represent NIST 3133 standard and middle peak represents MMHg standard.

Figure 3.9 shows the ^{202}Hg chromatogram for NIST 3133, along with the measured intensities of both thallium isotopes and the ratio of $^{205}Tl/^{203}Tl$. Although the individual thallium isotopes generate a variable signal, the ratio of the signals remains stable despite the fluctuations. The 10 ng/mL solution generated a combined Tl signal of ~10 V. All the standards analysed by GC contained a mass of ~500 pg of mercury species (either MMHg or inorganic mercury), generating a ^{202}Hg peak with maximum height between 2 – 2.5 V, which should be sufficient to calculate accurate and precise isotope ratios. For the traditional analysis of mercury isotope measurements, a peak height of at least 1 V is generally desirable for precise isotope ratio measurements (J. Liu et al., 2011). Initially, a few different masses of NIST 3133 were tested to test signal response. For 1000 pg, the peak height for ^{202}Hg was ~4 V, and for 300 pg, the peak height was between 1 – 1.5 V. Generally, a higher signal will result in more precise ratios, however the higher the concentration, the more likely for carryover between samples. Therefore, 500 pg was chosen as it produced a good signal, while being a low enough amount of mercury for carryover to not be as much of a concern.

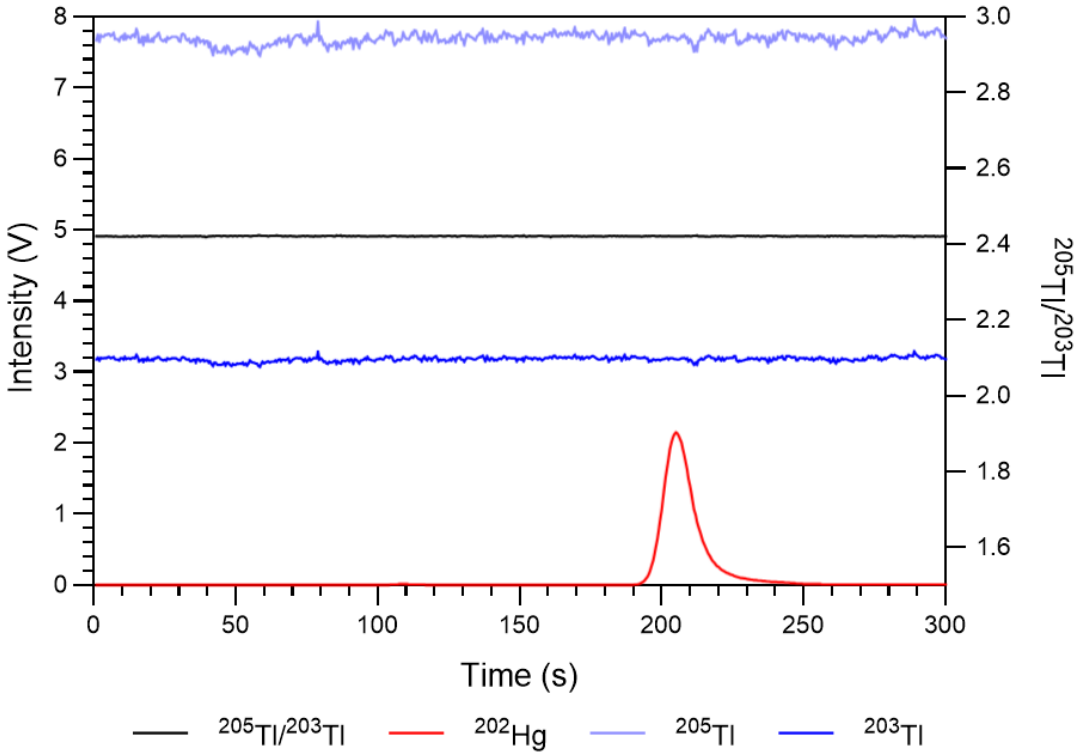

Figure 3.9. Chromatogram of ^{202}Hg including thallium isotopes and the $^{205}Tl/^{203}Tl$ signal simultaneously collected using MC-ICP-MS.

The isotope ratio of $^{202}Hg/^{198}Hg$ across the transient 3177 peak without baseline correction is illustrated in **Figure 3.10**. The isotope ratios are very high at the beginning an end of the peak but approaches a flat fairly consistent signal in the middle of the peak. **Figure 3.11** demonstrated the effect of baseline correction, with the measured intensities baseline corrected the ratios are much more consistent across the peak. Different amounts or percentages of the peak will result is different ratios, as a different number of data points is used depending on the percentage chosen. The selection of correct percentage of the peak is very important to obtain accurate and precise isotope ratios. To determine the best data treatment strategy, the four different baseline estimation methods, the three

different calculations methods, and the different percentages of the peak were compared using the NIST 3133 and 3177 standards (n=6).

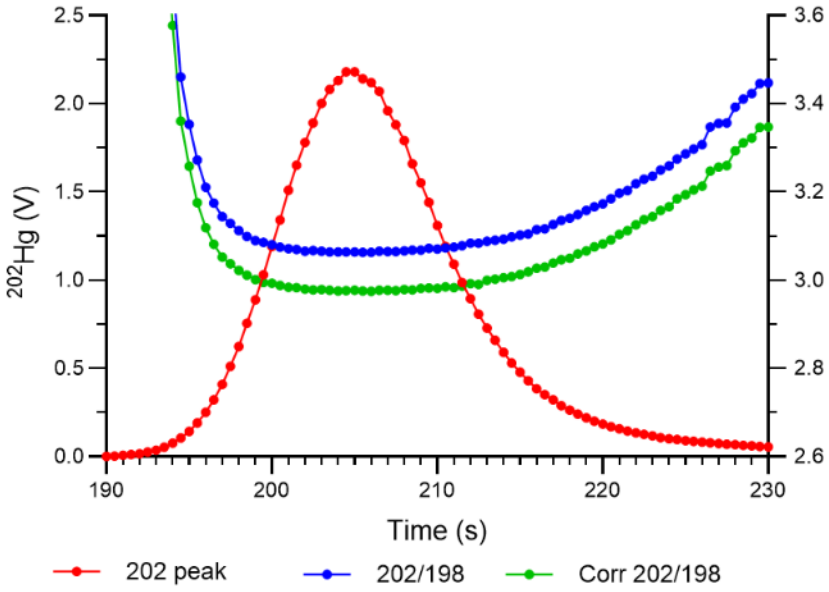

Figure 3.10. Calculated isotope ratios with no baseline correction of $^{202}Hg/^{198}Hg$ with and without thallium correction during NIST 3133 peak.

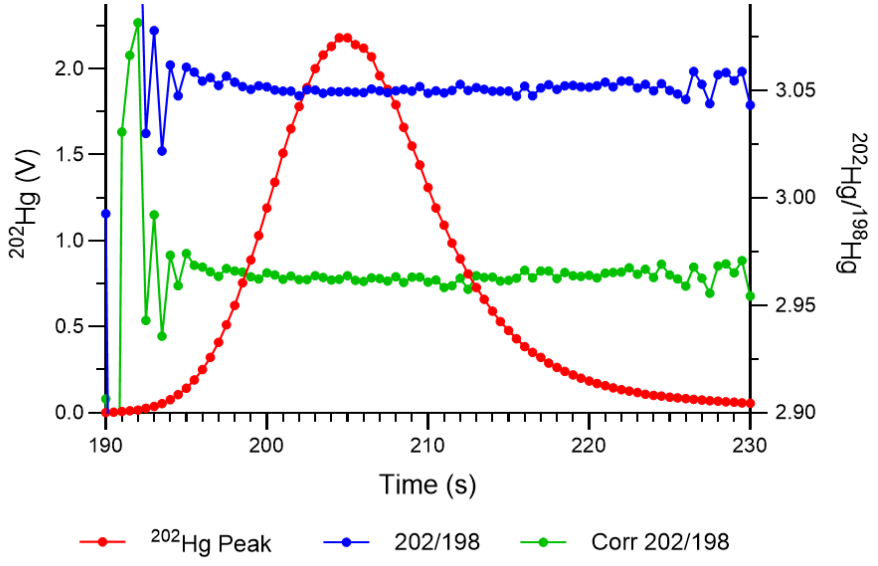

Figure 3.11. Baseline corrected isotope ratios of $^{202}Hg/^{198}Hg$ with and without thallium correction during NIST 3133 peak.

3.7.1. Data Treatment Strategies

The PBP method resulted in poor accuracy of the calculated isotope values using both a low percentage of the peak, 50%, and a high percentage of the peak, 95 and 100%. The high percentages of the peak also had very large standard deviations between the trials. The TopHat and median baseline methods gave the best results. The best accuracy and external precision were achieved using the TopHat baseline estimation method using 60% of the peak (δ^{202}Hg = – 0.50 ± 0.52‰, n=6) and using the median baseline method using 90% of the peak (δ^{202}Hg = – 0.60 ± 1.26‰, certified value = – 0.56 ± 0.03‰). The TopHat method gave more accurate and more precise ratios for all but δ^{200}Hg (– 0.60 ± 1.06‰, certified value – 0.27 ± 0.01‰). Overall, the PBP method gave the largest standard deviations of all the calculation methods.

The LRS method gave better results when more of the peak was included. This is consistent with Epov et al. (2010) who also found that including the background was important to achieve correct ratios using this method. There was very little difference between the calculated ratios using the different baseline estimation methods, which was expected because as the LRS method involves no baseline subtraction, the baseline estimation is only used for determining the bounds of the peak. The δ^{204}Hg and δ^{202}Hg ratios for 100% of the peak had good accuracy, however the average δ^{201}Hg, δ^{200}Hg and δ^{199}Hg were quite different from the certified value (**Table 3.6**), and the external precision was also worse.

Table 3.6. Isotope ratios of 3177 (n=6) calculated from 100% of the peak using LRS method with SNIP baseline correction method. Values corrected using thallium mass bias correction.

	δ^{204}	2SD	δ^{202}	2SD	δ^{201}	2SD	δ^{200}	2SD	δ^{199}	2SD
Measured	–0.80	0.55	–0.51	0.76	–0.67	1.09	–0.39	1.24	0.32	0.55
Certified	–0.82	0.07	–0.56	0.03	–0.46	0.02	–0.27	0.01	–0.17	0.01

The PAI method gave best accuracy and precision when using 80 – 95% of the peak. This is consistent with the results from Epov et al. (2008) who also found that using larger percentages of the peak increased the precision of the results. Using 100% of the peak, however, caused the accuracy and precision to decrease, likely because defining the beginning and end of the peak can be difficult to reproduce between peaks in different chromatograms, leading to areas that are not directly proportional to the peak ratio, and larger differences in calculated ratios between samples. The TopHat and median baseline estimation methods gave similar accuracy and precision, with the best method being the integration of 80% of the peak using the TopHat method for baseline estimation. Similar to the results using the LRS method, the δ^{204}Hg and δ^{202}Hg accuracy and precision is quite good, but the δ^{201}Hg and δ^{200}Hg had much larger uncertainty values, and δ^{199}Hg was quite different from the certified value (**Table 3.7**).

Table 3.7. Isotope ratios of 3177 (n=6) calculated by PAI using 80% of the peak with SNIP baseline correction method. Values corrected using thallium mass bias correction.

	δ^{204}	2SD	δ^{202}	2SD	δ^{201}	2SD	δ^{200}	2SD	δ^{199}	2SD
Measured	–0.78	0.44	–0.57	0.59	–0.55	0.90	–0.33	1.13	0.24	0.35
Certified	–0.82	0.07	–0.56	0.03	–0.46	0.02	–0.27	0.01	–0.17	0.01

Both the LRS method using 100% of the peak and the PAI using 80% of the peak gave similar results, however the PAI had slightly better accuracy and better precision and was chosen as the best calculation method. In all the calculation methods, the Tl correction did not greatly improve the results. **Table 3.8** shows a comparison between the chosen PAI method both with and without thallium correction. Neither method is clearly better than the other in terms of accuracy and precision for all isotopes. Given that previous studies have seen improved results using corrected ratios (Dzurko et al., 2009), the rest of the isotope ratios calculated in this research are reported using thallium correction.

Table 3.8. Comparison of 3177 (n=6) isotope ratios PAI using 80% of the peak with SNIP baseline correction method, with and without thallium mass bias correction.

	δ^{204}	2SD	δ^{202}	2SD	δ^{201}	2SD	δ^{200}	2SD	δ^{199}	2SD
Uncorrected	–0.81	0.57	–0.59	0.57	–0.56	0.81	–0.34	1.17	0.23	0.38
Corrected	–0.78	0.44	–0.57	0.59	–0.55	0.90	–0.33	1.13	0.24	0.35
Certified	–0.82	0.07	–0.56	0.03	–0.46	0.02	–0.27	0.01	–0.17	0.01
	Δ^{199}	2SD	Δ^{200}	2SD	Δ^{201}	2SD	Δ^{204}	2SD		
Uncorrected	0.38	0.15	–0.04	0.57	–0.12	0.45	0.07	0.47		
Corrected	0.38	0.15	–0.04	0.57	–0.12	0.45	–0.35	0.29		
Certified	–0.03	0.02	0.00	0.01	–0.04	0.01	0.00	0.02		

Figure 3.12 illustrates the differences between the measured and certified isotope ratios. Given the good accuracy of many of the isotope ratios, the difference between the measured and the certified value is likely not due to carryover of mercury between samples. To avoid contamination between the NIST 3133 and NIST 3177 samples, a water blank was run between the samples to clean the GC. This does have the drawback

of extending the time it takes to run the bracketing samples and the sample. The calculation of isotope ratios using the bracketing standard assumes that the instrument remains stable during the analysis of the bracketing standards and the sample. However, extending the time between when the first bracketing standard is measured and when the last bracketing standard is run could lead to inaccurate isotope ratios as the instrument response may change within that time. This could be contributing to the large uncertainty values associated with some of the measured delta values.

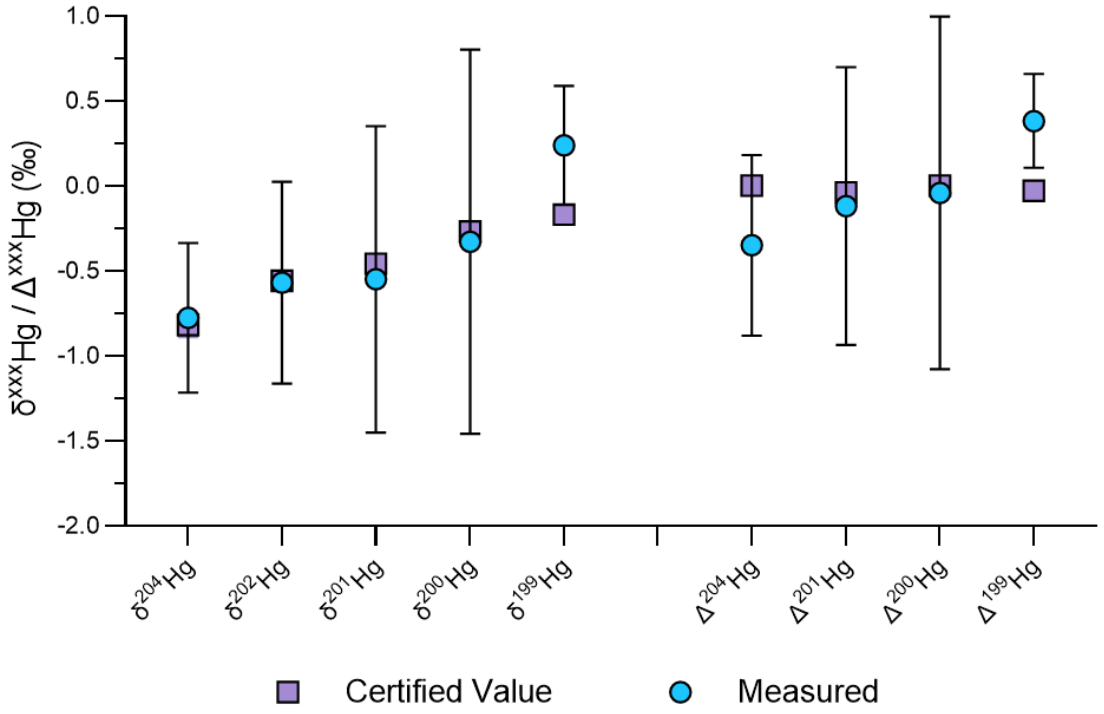

Figure 3.12. Measured isotope ratios of 3177 calculated by PAI of 80% of the peak using TopHat baseline estimation method versus the certified isotope ratio.

Another possible reason for poor accuracy of some of the isotope ratios may be due to the signal being too low, however if this were the case, it would be expected that the inaccuracy of the ratios would scale with the isotopic abundance. δ^{202}Hg being the most abundant, it makes sense that it had relatively high accuracy

($\delta^{202}Hg = -0.57 \pm 0.59‰$), however ^{204}Hg is the least abundant isotope measured, and it also had good accuracy ($\delta^{204}Hg = -0.77 \pm 0.44‰$), and ^{199}Hg being the third most abundant isotope had the worst accuracy ($\delta^{199}Hg = 0.24 \pm 0.80‰$).

Possibly, the large difference in $\delta^{199}Hg$ can be attributed to the use of enriched isotope material in our lab. A ^{199}Hg enriched material is routinely used by others in the lab as an internal standard during MMHg concentration analysis. These same samples are run through the Tekran® 2700, and since the ^{199}Hg abundance in the isotope enriched standard is much larger than the natural abundance, it may remain in the system and be eluted from the Tekran® during this research. ^{198}Hg and ^{200}Hg is also used in our lab to track mercury methylation and would be present at higher than its natural abundance in samples run through the Tekran®, which may be responsible for the large uncertainty. As well, Janssen et al. (2015) observed a positive MIF of ^{201}Hg and ^{199}Hg when the mercury vapour was passed through the CVAFS. They attributed this fractionation to the possible photochemical oxidation of elemental Hg or photoreduction of oxidized Hg deposited on the walls of the detector cell. This could be contributing to the large difference with certified value being observed in $\delta^{199}Hg$, however in this research a positive MIF was not observed for ^{201}Hg, rather the measured $\Delta^{201}Hg$ value was slightly more negative than the certified value. However, other research by (Mead et al., 2013) on mercury fractionation within fluorescent lamps found the MIF of ^{199}Hg and ^{201}Hg had opposite signs, which is more consistent with our results.

The external precision (2 SD) reported by previous online GC methods range between 0.33 – 0.56‰ (Bouchet et al., 2018; Dzurko et al., 2009; Epov et al., 2008, 2010; Queipo-Abad et al., 2019). The external precision measured in this research for

δ^{202}Hg was 0.59‰, which is not much larger than previous methods. The uncertainty for δ^{201}Hg (0.90‰) and δ^{200}Hg (1.13‰) remains quite large in comparison. Despite some isotopes having larger than desired uncertainties, all the measured ratios besides δ^{199}Hg were less than 0.1‰ different from the certified values, which is quite good, and the measured δ values were not statistically different from the certified values for all but δ^{199}Hg (one sample t-test, $p > 0.05$).

Figure 3.12 also displays the average MIF for the analysed standards. For Δ^{201}Hg and Δ^{200}Hg, the average values are very close to 0, similar to the certified value. Δ^{199}Hg has a positive MIF, which may be due to contamination from enriched Hg, or MIF within the GC. Δ^{204}Hg has a negative MIF, which may be due to lack of precision in the method since the uncertainty encompasses the certified value, but the m/z 204 may also be affected by the presence of ^{204}Pb. If ^{204}Pb was present in the sample, either from the water or reagents, it would be ethylated to $(C_2H_5)_4Pb$, which elutes with a very broad peak after the mercury species. Since the Tekran® 2700 is optimized for mercury species separation, the run time ends before $(C_2H_5)_4Pb$ is eluted, which would cause it to be eluted during the following sample chromatogram (Hintelmann & Evans, 1997). This would cause fluctuation in the measured m/z 204 and may be contributing to the variation in measured δ^{204}Hg that results in negative Δ^{204}Hg.

Future experiments are required to improve the accuracy and precision of this analysis method. Since the number of NIST 3177 samples measured using this method was small (n=6), additional sample are required to investigate whether the trends observed thus far are reproducible. Additionally, the possible contamination would need to be eliminated; this would likely require the use of a GC system that has never been

exposed to enriched isotopes. Also, bypassing the CVAFS detector should be tested to determine if it is imparting MIF on the samples. One additional parameter that could impact the accuracy is the integration time. An integration time of 0.5 seconds was used in this research based on the findings by (Queipo-Abad et al., 2019), who found that longer integration times were better for wide chromatographic peaks like the ones used in this research. Although, optimization of this parameter could improve results, it was not rigorously tested here, because the current method was not considered precise enough to draw any significant conclusions.

3.7.2. Isotope Ratio Measurement of MMHg

The standard MMHg solution was also analysed by GC-MC-ICP-MS, and the isotope ratios were calculated using the same method as described above. The standards were analysed using two different integration times, 0.5 sec and 1 sec. A comparison of the compound specific GC methods versus the directly measured MMHg stock solution, measuring MMHg as THg using the CV-system, is displayed in **Figure 3.13**. Statistically, none of the δ-values obtained through the compound specific GC analysis were significantly different from the directly measured stock MMHg values (one sample t-test, $p > 0.5$). In comparing the two integration times, neither gave obviously better accuracy or precision. The precision is better using 0.5 sec integration for the δ^{204}Hg, δ^{200}Hg, and δ^{199}g, but 1 sec integration gave better precision for δ^{202}Hg and δ^{201}Hg. As suggested previously, a more thorough investigation of many different integration methods would be required to determine the integration method that provides the highest accuracy and precision.

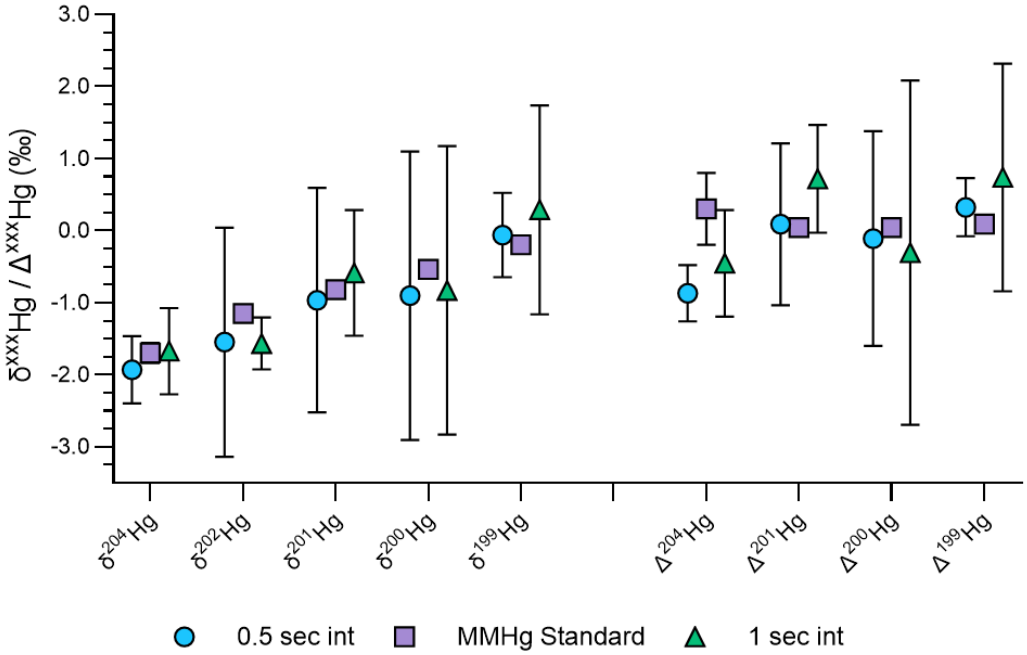

Figure 3.13. Measured isotope ratios of stock MMHg calculated by PAI of 80% of the peak using the TopHat baseline estimation method with integration time of 0.5 sec and 1 sec versus direct analysis of stock MMHg using CV-MC-ICP-MS.

Based on these results, MMHg isotope ratios from sediments with concentrations of MMHg as low as 0.1 ng/g could successfully be analysed. Potentially, sediments with MMHg concentrations as low as 0.06 ng/g could be analysed. From 5 g of sediment with this concentration, 300pg of MMHg would be extracted which would result in an instrument response of at least 1 V, which is the lowest desirable signal for accurate and precise isotope ratio measurement using the conventional CV sample introduction method. Additional study of various masses of MMHg using this method is required to determine the lowest concentration of MMHg in sediment that would result is accurate and precise isotope ratio measurements.

3.8. Analysis of Sediment Samples

Although the developed method would benefit from additional study to improve the precision to allow for the detection of differences in MMHg isotope ratios of samples, the field samples were still analysed to explore if the current strategy of sediment sample distillation followed by GC-MC-ICP-MS determination is viable form the analysis of MMHg isotope ratios in uncontaminated sediment samples.

3.8.1. THg Concentration Analysis

Difference in sediment THg concentrations is shown in **Figure 3.14** for three lakes in Kangiqsualujjuaq during winter and summer 2023. Replicates of the sediment samples varied only a little, with the relative standard deviations of samples ranging from 3.8 – 7.0%. Lake 5 had very little variation in concentration between seasons. Lake 11 in comparison, had a very large concentration difference between winter (16 ± 4 ng/g) and summer (58 ± 4 ng/g). Only one sediment core was taken from a single location in the lakes in both winter and summer. This apparent, large seasonal difference is likely due to the core samples being taken from different parts of the lake, rather than a significant loss of mercury in sediment during the winter. However, without additional samples from various locations in the lake, it is not possible to determine definitively the reason for this large seasonal variation. Lake 9 had a lower THg concentration in summer (36 ± 4 ng/g) in comparison to its neighboring, larger Lake 11 (58 ± 4 ng/g).

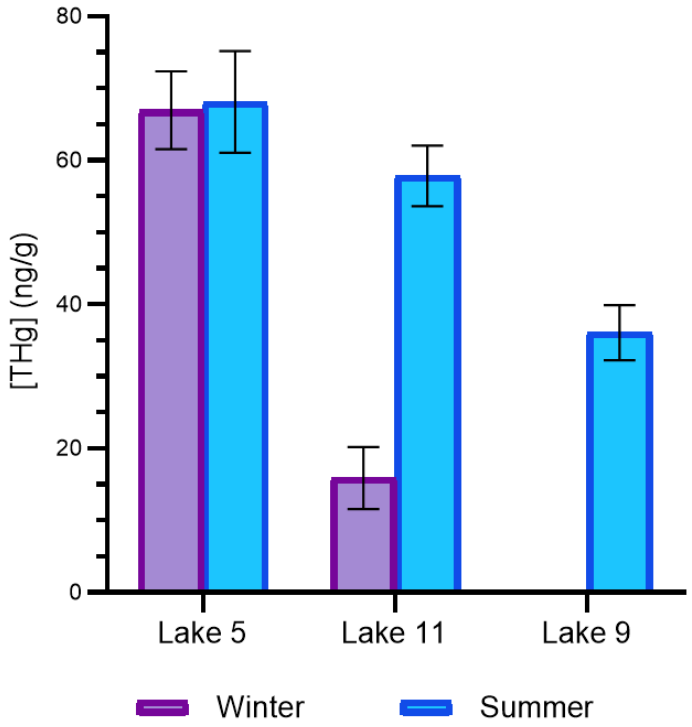

Figure 3.14. Concentration of THg in lakes.

3.8.2. THg Isotope Ratio Analysis of Sediment Samples

The range of isotopic compositions of the sediment samples is displayed in **Figure 3.15**. The differences between the δ^{202}Hg values between lakes are all statistically different ($p < 0.5$), and the δ^{202}Hg values between winter and summer for Lake 5 are also statistically significant. The 2 SD of sediment replicates range from 0.02 – 0.2‰. The graph of Δ^{199}Hg versus Δ^{201}Hg of the sediment samples has a line of best fit with a slope of 0.97 (**Figure 3.16**). A Δ^{199}Hg/Δ^{201}Hg ratio of 1.0 has been demonstrated by experimental studies to be a result of fractionation caused by the magnetic isotope effects during the photochemical reduction of Hg(II) (Bergquist & Blum, 2007). This fractionation may be responsible for the differences in the isotopic compositions of the

lakes in the summer and winter, since during the winter, the lakes are covered by a layer of ice and snow, so no photochemical reduction can occur.

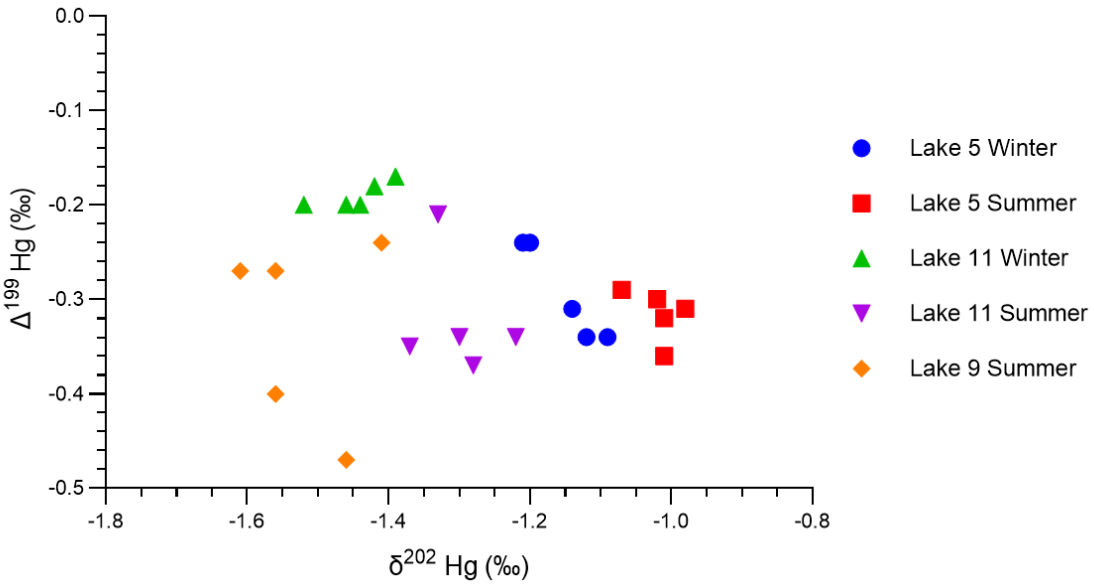

Figure 3.16. Plot of Δ^{199}Hg versus δ^{202}Hg for sediment samples.

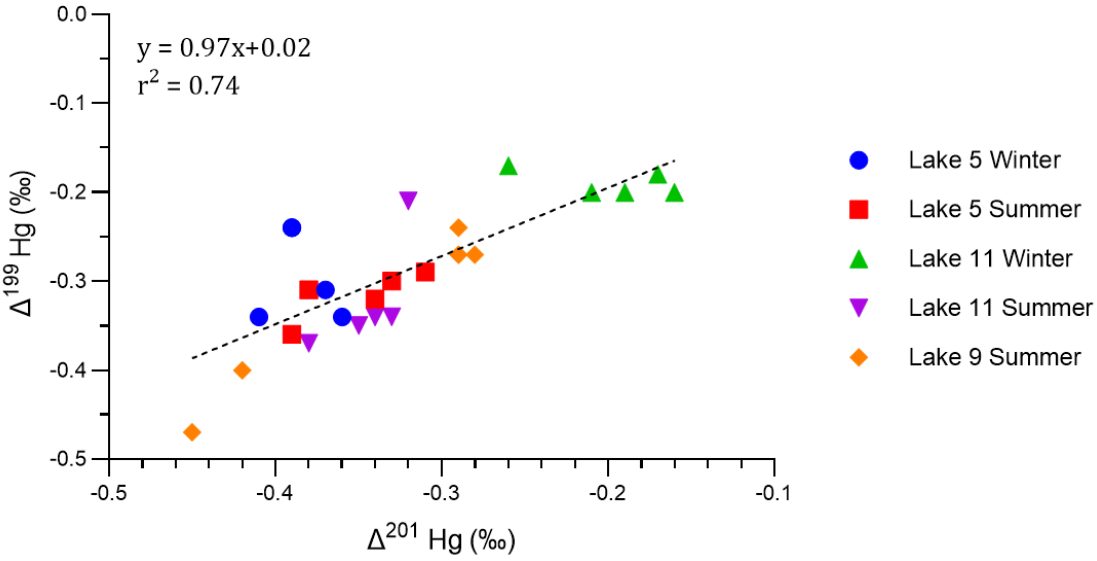

Figure 3.15. Plot of THg Δ^{201}Hg versus Δ^{199}Hg for sediment samples.

3.8.3. Species Specific Isotope Ratio Analysis of Samples

Figure 3.17 shows the measured isotopic compositions of distilled sediment samples. Three of the sediment samples were distilled in triplicate and measured using the developed method. The isotope ratios were calculated using the method determined previously. These results show that the developed method is able to successfully extract MMHg from the sediment samples, separate the difference species of mercury in the sample, and analyse the samples on the MC-ICP-MS. The analysis of three different subsamples of sediment, in addition to the uncertainty associated with the analysis method, resulted in very large external precision for the measured isotope ratios. The average δ values do suggest negative fractionation in the isotope ratios during incubation, but with such large uncertainty values, it is not possible to draw any definitive conclusion from this data.

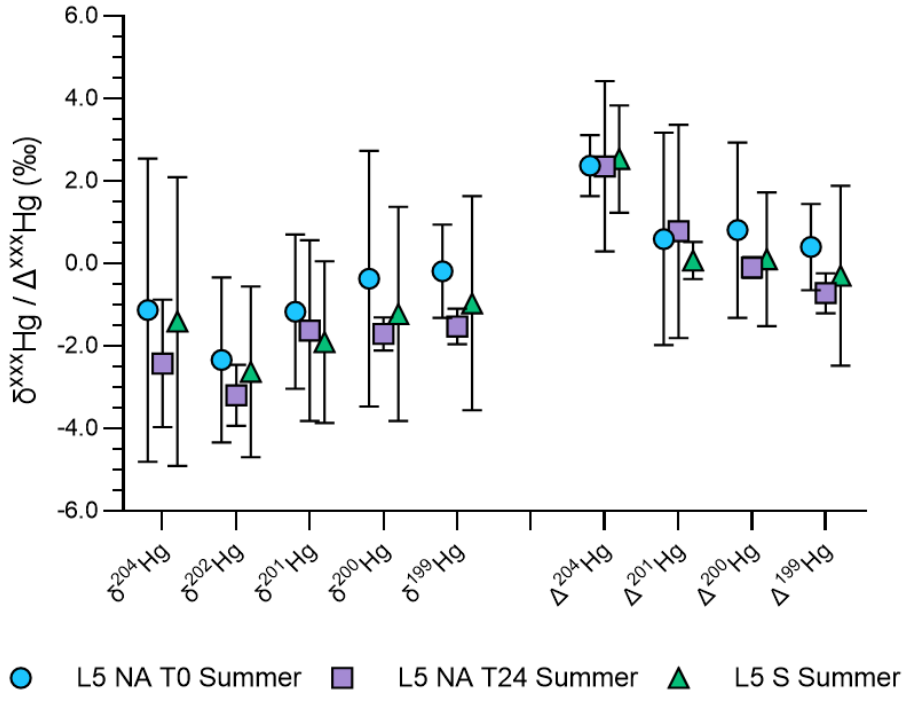

Figure 3.17. Isotopic composition of sediment samples.

Chapter 4: Conclusion

Isotope ratio analysis of mercury is used to trace the movement and biogeochemical transformations of mercury in the environment. Since MMHg is the most toxic form of mercury, there is great interest in measuring species specific isotope compositions of MMHg, to better understand its cycling and to limit human exposure. This research presents a method to measure MMHg isotope ratios and associated isotope fractionation using MC-ICP-MS. First, an extraction method was developed to extract MMHg from sediment using distillation. The extraction method had good recovery at 96 ± 10% and can be scaled up to effectively extract MMHg from up to 5 grams of sediment. The method was also evaluated to ensure it does not impart any isotope fractionation to MMHg present in the sediment samples. No isotope fractionation was observed in full distillations of the stock MMHg standard or in any fraction of the distillation. Distillation of MMHg from a real sample was also tested using BCR 464 (tuna fish) and no fractionation was observed.

The Tekran® 2700 automated MMHg analyzer was successfully coupled to the MC-ICP-MS and the various data treatment strategies were explored to obtain most accurate and precise results. The calculations were facilitated using IsoCor, a data processing application. Of the three calculation methods, the point-by-point (PBP) method had the largest uncertainties. The linear regression slope (LRS) and peak area integration (PAI) methods gave similar results, with the PAI giving the most precise results when using the TopHat baseline correction method and integrating 80% of the peak. Applying the developed methodology to NIST 3177, a standard mercury solution, resulted in measured $\delta^{202}Hg = -0.57 \pm 0.59‰$. Although this precision (2 SD) is not

much larger than the precision reported by previous studies, some of the other isotope ratios did have larger uncertainty values. However, the δ of all the measured isotope ratios, except for $\delta^{199}Hg$ were statistically not different from certified values.

Although additional research to improve the precision of the method is required before being able to detect small differences among real samples, this method already possesses some notable strengths. First, the overall method from extraction to analysis is relatively quick and straightforward in comparison to other methods, namely offline methods. Only distillation is required for sample processing which takes 2 – 3 h, in comparison to the multi-step offline methods (Janssen et al., 2015; Qin et al., 2018; Rosera et al., 2020), which could take many days the process samples. This method also has the advantage that it is sensitive enough for the analysis of sediments with background levels of MMHg, rather than being limited to only contaminated sediments, which is the case for many of the previous methods.

Initial analysis of THg isotope ratios of the sediment samples from thermokarst lakes in Kangiqsualujjuaq found statistically significant differences in the isotopic compositions between lakes and between seasons for Lake 5. The $\Delta^{199}Hg/\Delta^{201}Hg$ relationship in the sediment samples suggests that the observed MIF is caused by magnetic isotope effects during the photochemical reduction of Hg(II). This method can successfully measure isotope ratios of MMHg in samples with concentrations as low as 0.1 ng/g but is currently not precise enough to distinguish differences in the MMHg isotopic composition of real samples. These results suggest that with additional precision, the method could be applied to the Kangiqsualujjuaq sediment samples to add to our general understanding of MMHg in thermokarst lakes.

Future studies are needed to reduce the large uncertainty currently associated with the method. A larger sample size of standards should be measured to make more concrete conclusions about the accuracy and precision of the method. Additionally, samples should be analysed by bypassing the CVAFS to determine if any MIF is occurring in the fluorescence cell. Finally, once validated, a more precise method could be applied to the sediment samples to determine what effect the amendments and incubations had on the isotopic composition of MMHg in the samples.

This research provides a way of studying MMHg which can be used to broaden our understanding of MMHg cycling in the environment. The results demonstrated that an online GC method is the most feasible method to be able to analyse MMHg isotope ratios of samples with background concentration of MMHg, as the GC is able to concentrate the mass of MMHg prior to introduction to the MC-ICP-MS. This approach can be tested in the future for the isotope ratio analysis of MMHg in other environmental sample types. For example, the use of online GC could be investigated for the analysis of MMHg isotope ratios in water, which has very low MMHg concentrations, even lower than sediment. The developed method can be applied to a broad range of sediments samples with various MMHg concentrations, as samples only require a concentration of 0.1 ng/g to be analysed using this method. This will allow for the analysis of the transformations of mercury that occur during both methylation and demethylation. Overall, this study presents a valuable approach to studying MMHg isotope ratios, an emerging area of research that is critical to advancing our understanding of mercury in the environment.

References

Acquavita, A., Floreani, F., & Covelli, S. (2021). Occurrence and speciation of arsenic and mercury in alluvial and coastal sediments. *Current Opinion in Environmental Science & Health*, *22*, 100272. https://doi.org/10.1016/j.coesh.2021.100272

Ahmed, R., & Stoeppler, M. (1987). Storage and stability of mercury and methylmercury in sea water. *Analytica Chimica Acta*, *192*, 109–113. https://doi.org/10.1016/S0003-2670(00)85693-7

AMAP, 2021. AMAP Assessment 2021: Mercury in the Arctic. Arctic Monitoring and Assessment Programme (AMAP), Tromsø, Norway.

Avramescu, M., Zhu, J., Yumvihoze, E., Hintelmann, H., Fortin, D., & Lean, D. R. S. (2010). Simplified sample preparation procedure for measuring isotope-enriched methylmercury by gas chromatography and inductively coupled plasma mass spectrometry. *Environmental Toxicology and Chemistry*, *29*(6), 1256–1262. https://doi.org/10.1002/etc.158

Barkay, T., & Gu, B. (2022). Demethylation─The Other Side of the Mercury Methylation Coin: A Critical Review. *ACS Environmental Au*, *2*(2), 77–97. https://doi.org/10.1021/acsenvironau.1c00022

Bento, B., & Hintelmann, H. (2024). Assessment of mercury methylation and methylmercury demethylation potentials in water and sediments along the Wabigoon River system. *Science of The Total Environment*, *951*, 175658. https://doi.org/10.1016/j.scitotenv.2024.175658

Bergquist, B. A., & Blum, J. D. (2007). Mass-Dependent and -Independent Fractionation of Hg Isotopes by Photoreduction in Aquatic Systems. *Science*, *318*(5849), 417–420. https://doi.org/10.1126/science.1148050

Bettoso, N., Pittaluga, F., Predonzani, S., Zanello, A., & Acquavita, A. (2023). Mercury Levels in Sediment, Water and Selected Organisms Collected in a Coastal Contaminated Environment: The Marano and Grado Lagoon (Northern Adriatic Sea, Italy). *Applied Sciences*, *13*(5), 3064. https://doi.org/10.3390/app13053064

Bigeleisen, J. (1996). Nuclear Size and Shape Effects in Chemical Reactions. Isotope Chemistry of the Heavy Elements. *Journal of the American Chemical Society*, *118*(15), 3676–3680. https://doi.org/10.1021/ja954076k

Black, F. J., Conaway, C. H., & Flegal, A. R. (2009). Stability of Dimethyl Mercury in Seawater and Its Conversion to Monomethyl Mercury. *Environmental Science & Technology*, *43*(11), 4056–4062. https://doi.org/10.1021/es9001218

Bloom, N. S., Colman, J. A., & Barber, L. (1997). Artifact formation of methyl mercury during aqueous distillation and alternative techniques for the extraction of methyl mercury from environmental samples. *Fresenius' Journal of Analytical Chemistry*, *358*(3), 371–377. https://doi.org/10.1007/s002160050432

Blum, J. D. (2011). Applications of stable mercury isotopes to biogeochemistry. In M, Baskaran (Ed.). *Handbook of environmental isotope geochemistry (ed*., 229-246). London, New York: Springer.

Blum, J. D., & Bergquist, B. A. (2007). Reporting of variations in the natural isotopic composition of mercury. *Analytical and Bioanalytical Chemistry*, *388*(2), 353–359. https://doi.org/10.1007/s00216-007-1236-9

Blum, J. D., & Johnson, M. W. (2017). Recent Developments in Mercury Stable Isotope Analysis. *Reviews in Mineralogy and Geochemistry*, *82*(1), 733–757. https://doi.org/10.2138/rmg.2017.82.17

Borge, A. F., Westermann, S., Solheim, I., & Etzelmüller, B. (2017). Strong degradation of palsas and peat plateaus in northern Norway during the last 60 years. *The Cryosphere*, *11*(1), 1–16. https://doi.org/10.5194/tc-11-1-2017

Bouchet, S., Bérail, S., & Amouroux, D. (2018). Hg Compound-Specific Isotope Analysis at Ultratrace Levels Using an on Line Gas Chromatographic Preconcentration and Separation Strategy Coupled to Multicollector-Inductively Coupled Plasma Mass Spectrometry. *Analytical Chemistry*, *90*(13), 7809–7816. https://doi.org/10.1021/acs.analchem.7b04555

Bussan, D. D., Douvris, C., & Cizdziel, J. V. (2022). Mercury Methylation Potentials in Sediments of an Ancient Cypress Wetland Using Species-Specific Isotope Dilution GC-ICP-MS. *Molecules*, *27*(15), 4911. https://doi.org/10.3390/molecules27154911

Cai, H., & Chen, J. (2016). Mass-independent fractionation of even mercury isotopes. *Science Bulletin*, *61*(2), 116–124. https://doi.org/10.1007/s11434-015-0968-8

Chang, L. W. (1977). Neurotoxic effects of mercury—A review. *Environmental Research*, *14*(3), 329–373. https://doi.org/10.1016/0013-9351(77)90044-5

Chen, J., Hintelmann, H., & Dimock, B. (2010). Chromatographic pre-concentration of Hg from dilute aqueous solutions for isotopic measurement by MC-ICP-MS. *Journal of Analytical Atomic Spectrometry*, *25*(9), 1402. https://doi.org/10.1039/c0ja00014k

Chen, J., Hintelmann, H., Feng, X., & Dimock, B. (2012). Unusual fractionation of both odd and even mercury isotopes in precipitation from Peterborough, ON, Canada. *Geochimica et Cosmochimica Acta*, *90*, 33–46. https://doi.org/10.1016/j.gca.2012.05.005

Clayden, M. G., Kidd, K. A., Wyn, B., Kirk, J. L., Muir, D. C. G., & O'Driscoll, N. J. (2013). Mercury Biomagnification through Food Webs Is Affected by Physical and Chemical Characteristics of Lakes. *Environmental Science & Technology*, *47*(21), 12047–12053. https://doi.org/10.1021/es4022975

Crowther, E. R., Demers, J. D., Blum, J. D., Brooks, S. C., & Johnson, M. W. (2023). Coupling of nitric acid digestion and anion-exchange resin separation for the determination of methylmercury isotopic composition within organisms. *Analytical and Bioanalytical Chemistry*, *415*(5), 759–774. https://doi.org/10.1007/s00216-022-04468-8

Demers, J. D., Blum, J. D., & Zak, D. R. (2013). Mercury isotopes in a forested ecosystem: Implications for air-surface exchange dynamics and the global mercury cycle. *Global Biogeochemical Cycles*, *27*(1), 222–238. https://doi.org/10.1002/gbc.20021

Donovan, P. M., Blum, J. D., Singer, M. B., Marvin-DiPasquale, M., & Tsui, M. T. K. (2016). Isotopic Composition of Inorganic Mercury and Methylmercury Downstream of a Historical Gold Mining Region. *Environmental Science & Technology*, *50*(4), 1691–1702. https://doi.org/10.1021/acs.est.5b04413

Durnford, D., Dastoor, A., Figueras-Nieto, D., & Ryjkov, A. (2010). Long range transport of mercury to the Arctic and across Canada. *Atmospheric Chemistry and Physics*, *10*(13), 6063–6086. https://doi.org/10.5194/acp-10-6063-2010

Dzurko, M., Foucher, D., & Hintelmann, H. (2009). Determination of compound-specific Hg isotope ratios from transient signals using gas chromatography coupled to multicollector inductively coupled plasma mass spectrometry (MC-ICP/MS). *Analytical and Bioanalytical Chemistry*, *393*(1), 345–355. https://doi.org/10.1007/s00216-008-2165-y

Engstrom, D. R. (2007). Fish respond when the mercury rises. *Proceedings of the National Academy of Sciences*, *104*(42), 16394–16395. https://doi.org/10.1073/pnas.0708273104

Epov, V. N., Berail, S., Jimenez-Moreno, M., Perrot, V., Pecheyran, C., Amouroux, D., & Donard, O. F. X. (2010). Approach to Measure Isotopic Ratios in Species Using Multicollector-ICPMS Coupled with Chromatography. *Analytical Chemistry*, *82*(13), 5652–5662. https://doi.org/10.1021/ac100648f

Epov, V. N., Berail, S., Pécheyran, C., Amouroux, D., & Donard, O. F. X. (2012). Isotopic Analysis via Multi-Collector Inductively Coupled Plasma Mass Spectrometry in Elemental Speciation. In *Isotopic Analysis* (pp. 495–517). John Wiley & Sons, Ltd. https://doi.org/10.1002/9783527650484.ch17

Epov, V. N., Rodriguez-Gonzalez, P., Sonke, J. E., Tessier, E., Amouroux, D., Bourgoin, L. M., & Donard, O. F. X. (2008). Simultaneous Determination of Species-Specific Isotopic Composition of Hg by Gas Chromatography Coupled to Multicollector ICPMS. *Analytical Chemistry*, *80*(10), 3530–3538. https://doi.org/10.1021/ac800384b

Eriksen, H. H., & Perrez, F. X. (2014). The Minamata Convention: A Comprehensive Response to a Global Problem. *Review of European, Comparative & International Environmental Law*, *23*(2), 195–210. https://doi.org/10.1111/reel.12079

Evans, R. D., Hintelmann, H., & Dillon, P. J. (2001). Measurement of high precision isotope ratios for mercury from coals using transient signals. *Journal of Analytical Atomic Spectrometry*, *16*(9), 1064–1069. https://doi.org/10.1039/b103247j

Feng, C., Pedrero, Z., Lima, L., Olivares, S., De La Rosa, D., Berail, S., Tessier, E., Pannier, F., & Amouroux, D. (2019). Assessment of Hg contamination by a Chlor-Alkali Plant in riverine and coastal sites combining Hg speciation and isotopic signature (Sagua la Grande River, Cuba). *Journal of Hazardous Materials*, *371*, 558–565. https://doi.org/10.1016/j.jhazmat.2019.02.092

Feng, X., Foucher, D., Hintelmann, H., Yan, H., He, T., & Qiu, G. (2010). Tracing Mercury Contamination Sources in Sediments Using Mercury Isotope Compositions. *Environmental Science & Technology*, *44*(9), 3363–3368. https://doi.org/10.1021/es9039488

Fietzke, J., Liebetrau, V., Günther, D., Gürs, K., Hametner, K., Zumholz, K., Hansteen, T. H., & Eisenhauer, A. (2008). An alternative data acquisition and evaluation

strategy for improved isotope ratio precision using LA-MC-ICP-MS applied to stable and radiogenic strontium isotopes in carbonates. *Journal of Analytical Atomic Spectrometry*, *23*(7), 955. https://doi.org/10.1039/b717706b

Gray, J. E., Van Metre, P. C., Pribil, M. J., & Horowitz, A. J. (2015). Tracing historical trends of Hg in the Mississippi River using Hg concentrations and Hg isotopic compositions in a lake sediment core, Lake Whittington, Mississippi, USA. *Chemical Geology*, *395*, 80–87. https://doi.org/10.1016/j.chemgeo.2014.12.005

Gworek, B., Dmuchowski, W., & Baczewska-Dąbrowska, A. H. (2020). Mercury in the terrestrial environment: A review. *Environmental Sciences Europe*, *32*(1), 128. https://doi.org/10.1186/s12302-020-00401-x

Hammerschmidt, C. R., Fitzgerald, W. F., Lamborg, C. H., Balcom, P. H., & Tseng, C.-M. (2006). Biogeochemical Cycling of Methylmercury in Lakes and Tundra Watersheds of Arctic Alaska. *Environmental Science & Technology*, *40*(4), 1204–1211. https://doi.org/10.1021/es051322b

Harrington, C. F., Merson, S. A., & D' Silva, T. M. (2004). Method to reduce the memory effect of mercury in the analysis of fish tissue using inductively coupled plasma mass spectrometry. *Analytica Chimica Acta*, *505*(2), 247–254. https://doi.org/10.1016/j.aca.2003.10.046

Heginbottom, J. A. (2002). Permafrost mapping: A review. *Progress in Physical Geography: Earth and Environment*, *26*(4), 623–642. https://doi.org/10.1191/0309133302pp355ra

Hintelmann, H. (2012). Use of Stable Isotopes in Mercury Research. In M. Bank (Ed.), *Mercury in the Environment* (pp. 55–72). University of California Press. https://doi.org/10.1525/california/9780520271630.003.0004

Hintelmann, H., & Evans, R. D. (1997). Application of stable isotopes in environmental tracer studies—Measurement of monomethylmercury (CH 3 Hg +) by isotope dilution ICP-MS and detection of species transformation. *Fresenius' Journal of Analytical Chemistry*, *358*(3), 378–385. https://doi.org/10.1007/s002160050433

Hintelmann, H., & Zheng, W. (2011). Tracking Geochemical Transformations and Transport of Mercury through Isotope Fractionation. In G. Liu, Y. Cai, & N. O'Driscoll (Eds.), *Environmental Chemistry and Toxicology of Mercury* (pp. 293–327). John Wiley & Sons, Inc. https://doi.org/10.1002/9781118146644.ch9

Hong, Y.-S., Kim, Y.-M., & Lee, K.-E. (2012). Methylmercury Exposure and Health Effects. *Journal of Preventive Medicine & Public Health*, *45*(6), 353–363. https://doi.org/10.3961/jpmph.2012.45.6.353

Horvat, M., Bloom, N. S., & Liang, L. (1993). Comparison of distillation with other current isolation methods for the determination of methyl mercury compounds in low level environmental samples. *Analytica Chimica Acta*, *281*(1), 135–152. https://doi.org/10.1016/0003-2670(93)85348-N

Ignatavičius, G., Unsal, M. H., Busher, P. E., Wołkowicz, S., Satkūnas, J., Šulijienė, G., & Valskys, V. (2022). Geochemistry of mercury in soils and water sediments. *AIMS Environmental Science*, *9*(3), 277–297. https://doi.org/10.3934/environsci.2022019

Ingle, C. P., Sharp, B. L., Horstwood, M. S. A., Parrish, R. R., & Lewis, D. J. (2003). Instrument response functions, mass bias and matrix effects in isotope ratio measurements and semi-quantitative analysis by single and multi-collector ICP-MS. *Journal of Analytical Atomic Spectrometry*, *18*(3), 219–229. https://doi.org/10.1039/b211527a

Janssen, S. E., Johnson, M. W., Blum, J. D., Barkay, T., & Reinfelder, J. R. (2015). Separation of monomethylmercury from estuarine sediments for mercury isotope analysis. *Chemical Geology*, *411*, 19–25. https://doi.org/10.1016/j.chemgeo.2015.06.017

Jeremiason, J. D., Engstrom, D. R., Swain, E. B., Nater, E. A., Johnson, B. M., Almendinger, J. E., Monson, B. A., & Kolka, R. K. (2006). Sulfate Addition Increases Methylmercury Production in an Experimental Wetland. *Environmental Science & Technology*, *40*(12), 3800–3806. https://doi.org/10.1021/es0524144

Jiménez-Moreno, M., Perrot, V., Epov, V. N., Monperrus, M., & Amouroux, D. (2013). Chemical kinetic isotope fractionation of mercury during abiotic methylation of Hg(II) by methylcobalamin in aqueous chloride media. *Chemical Geology*, *336*, 26–36. https://doi.org/10.1016/j.chemgeo.2012.08.029

Kessler, R. (2013). The Minamata Convention on Mercury: A First Step toward Protecting Future Generations. *Environmental Health Perspectives*, *121*(10). https://doi.org/10.1289/ehp.121-A304

Kirk, J. L., Lehnherr, I., Andersson, M., Braune, B. M., Chan, L., Dastoor, A. P., Durnford, D., Gleason, A. L., Loseto, L. L., Steffen, A., & St. Louis, V. L. (2012). Mercury in Arctic marine ecosystems: Sources, pathways and exposure.

Environmental Research, *119*, 64–87. https://doi.org/10.1016/j.envres.2012.08.012

Kritee, K., Blum, J. D., & Barkay, T. (2008). Mercury Stable Isotope Fractionation during Reduction of Hg(II) by Different Microbial Pathways. *Environmental Science & Technology*, *42*(24), 9171–9177. https://doi.org/10.1021/es801591k

Krupp, E. M., & Donard, O. F. X. (2005). Isotope ratios on transient signals with GC–MC–ICP-MS. *International Journal of Mass Spectrometry*, *242*(2–3), 233–242. https://doi.org/10.1016/j.ijms.2004.11.026

Kumar, N. (Ed.). (2024). *Mercury Toxicity Mitigation: Sustainable Nexus Approach*. Springer Nature Switzerland. https://doi.org/10.1007/978-3-031-48817-7

Lehnherr, I., St. Louis, V. L., Emmerton, C. A., Barker, J. D., & Kirk, J. L. (2012). Methylmercury Cycling in High Arctic Wetland Ponds: Sources and Sinks. *Environmental Science & Technology*, *46*(19), 10514–10522. https://doi.org/10.1021/es300576p

Lehnherr, I., St. Louis, V. L., & Kirk, J. L. (2012). Methylmercury Cycling in High Arctic Wetland Ponds: Controls on Sedimentary Production. *Environmental Science & Technology*, *46*(19), 10523–10531. https://doi.org/10.1021/es300577e

Li, F., Ma, C., & Zhang, P. (2020). Mercury Deposition, Climate Change and Anthropogenic Activities: A Review. *Frontiers in Earth Science*, *8*, 316. https://doi.org/10.3389/feart.2020.00316

Lindberg, S. E., & Stratton, W. J. (1998). Atmospheric Mercury Speciation: Concentrations and Behavior of Reactive Gaseous Mercury in Ambient Air. *Environmental Science & Technology*, *32*(1), 49–57. https://doi.org/10.1021/es970546u

Liu, G., Cai, Y., & O'Driscoll, N. J. (Eds.). (2012). *Environmental chemistry and toxicology of mercury*. Wiley.

Liu, J., Feng, X., Yin, R., Zhu, W., & Li, Z. (2011). Mercury distributions and mercury isotope signatures in sediments of Dongjiang, the Pearl River Delta, China. *Chemical Geology*, *287*(1–2), 81–89. https://doi.org/10.1016/j.chemgeo.2011.06.001

Macdonald, R. W., Barrie, L. A., Bidleman, T. F., Diamond, M. L., Gregor, D. J., Semkin, R. G., Strachan, W. M. J., Li, Y. F., Wania, F., Alaee, M., Alexeeva, L. B., Backus, S. M., Bailey, R., Bewers, J. M., Gobeil, C., Halsall, C. J., Harner, T.,

Hoff, J. T., Jantunen, L. M. M., … Yunker, M. B. (2000). Contaminants in the Canadian Arctic: 5 years of progress in understanding sources, occurrence and pathways. *Science of The Total Environment*, *254*(2–3), 93–234. https://doi.org/10.1016/S0048-9697(00)00434-4

Mansfield, C. R., & Black, F. J. (2015). Quantification of monomethylmercury in natural waters by direct ethylation: Interference characterization and method optimization. *Limnology and Oceanography: Methods*, *13*(2), 81–91. https://doi.org/10.1002/lom3.10009

Marvin-DiPasquale, M., Agee, J., McGowan, C., Oremland, R. S., Thomas, M., Krabbenhoft, D., & Gilmour, C. C. (2000). Methyl-Mercury Degradation Pathways: A Comparison among Three Mercury-Impacted Ecosystems. *Environmental Science & Technology*, *34*(23), 4908–4916. https://doi.org/10.1021/es0013125

Masbou, J., Point, D., & Sonke, J. E. (2013). Application of a selective extraction method for methylmercury compound specific stable isotope analysis (MeHg-CSIA) in biological materials. *Journal of Analytical Atomic Spectrometry*, *28*(10), 1620. https://doi.org/10.1039/c3ja50185j

Mason, R. P., & Fitzgerald, W. F. (1993). The distribution and biogeochemical cycling of mercury in the equatorial Pacific Ocean. *Deep Sea Research Part I: Oceanographic Research Papers*, *40*(9), 1897–1924. https://doi.org/10.1016/0967-0637(93)90037-4

Mason, R., & Pirrone, N. (Eds.). (2009). *Mercury Fate and Transport in the Global Atmosphere: Emissions, Measurements and Models*. Springer US. https://doi.org/10.1007/978-0-387-93958-2

Mead, C., Lyons, J. R., Johnson, T. M., & Anbar, A. D. (2013). Unique Hg Stable Isotope Signatures of Compact Fluorescent Lamp-Sourced Hg. *Environmental Science & Technology*, *47*(6), 2542–2547. https://doi.org/10.1021/es303940p

Method 1630: Methyl Mercury in Water by Distillation, Aqueous Ethylation, Purge and Trap, and Cold Vapor Atomic Fluorescence Spectrometry. (1998).

Miller, E. K., Vanarsdale, A., Keeler, G. J., Chalmers, A., Poissant, L., Kamman, N. C., & Brulotte, R. (2005). Estimation and Mapping of Wet and Dry Mercury Deposition Across Northeastern North America. *Ecotoxicology*, *14*(1–2), 53–70. https://doi.org/10.1007/s10646-004-6259-9

O'Connor, D., Hou, D., Ok, Y. S., Mulder, J., Duan, L., Wu, Q., Wang, S., Tack, F. M. G., & Rinklebe, J. (2019). Mercury speciation, transformation, and transportation in soils, atmospheric flux, and implications for risk management: A critical review. *Environment International*, *126*, 747–761. https://doi.org/10.1016/j.envint.2019.03.019

Olson, C., Jiskra, M., Biester, H., Chow, J., & Obrist, D. (2018). Mercury in Active-Layer Tundra Soils of Alaska: Concentrations, Pools, Origins, and Spatial Distribution. *Global Biogeochemical Cycles*, *32*(7), 1058–1073. https://doi.org/10.1029/2017GB005840

Oremland, R. S., Culbertson, C. W., & Winfrey, M. R. (1991). Methylmercury Decomposition in Sediments and Bacterial Cultures: Involvement of Methanogens and Sulfate Reducers in Oxidative Demethylation. *Applied and Environmental Microbiology*, *57*(1), 130–137. https://doi.org/10.1128/aem.57.1.130-137.1991

Oyekola, O. O., Van Hille, R. P., & Harrison, S. T. L. (2009). Study of anaerobic lactate metabolism under biosulfidogenic conditions. *Water Research*, *43*(14), 3345–3354. https://doi.org/10.1016/j.watres.2008.11.044

Paffrath, R., Laukert, G., Bauch, D., Rutgers Van Der Loeff, M., & Pahnke, K. (2021). Separating individual contributions of major Siberian rivers in the Transpolar Drift of the Arctic Ocean. *Scientific Reports*, *11*(1), 8216. https://doi.org/10.1038/s41598-021-86948-y

Perez, P. A., Hintelman, H., Quiroz, W., & Bravo, M. A. (2017). Critical evaluation of distillation procedure for the determination of methylmercury in soil samples. *Chemosphere*, *186*, 570–575. https://doi.org/10.1016/j.chemosphere.2017.08.034

Perrot, V., Bridou, R., Pedrero, Z., Guyoneaud, R., Monperrus, M., & Amouroux, D. (2015). Identical Hg Isotope Mass Dependent Fractionation Signature during Methylation by Sulfate-Reducing Bacteria in Sulfate and Sulfate-Free Environment. *Environmental Science & Technology*, *49*(3), 1365–1373. https://doi.org/10.1021/es5033376

Perrot, V., Masbou, J., Pastukhov, M. V., Epov, V. N., Point, D., Bérail, S., Becker, P. R., Sonke, J. E., & Amouroux, D. (2016). Natural Hg isotopic composition of different Hg compounds in mammal tissues as a proxy for in vivo breakdown of toxic methylmercury. *Metallomics*, *8*(2), 170–178. https://doi.org/10.1039/C5MT00286A

Pietilä, H., Perämäki, P., Piispanen, J., Starr, M., Nieminen, T., Kantola, M., & Ukonmaanaho, L. (2015). Determination of low methylmercury concentrations in peat soil samples by isotope dilution GC-ICP-MS using distillation and solvent extraction methods. *Chemosphere*, *124*, 47–53. https://doi.org/10.1016/j.chemosphere.2014.11.001

Pirrone, N., Cinnirella, S., Feng, X., Finkelman, R. B., Friedli, H. R., Leaner, J., Mason, R., Mukherjee, A. B., Stracher, G. B., Streets, D. G., & Telmer, K. (2010). Global mercury emissions to the atmosphere from anthropogenic and natural sources. *Atmospheric Chemistry and Physics*, *10*(13), 5951–5964. https://doi.org/10.5194/acp-10-5951-2010

Poulin, B. A., Janssen, S. E., Rosera, T. J., Krabbenhoft, D. P., Eagles-Smith, C. A., Ackerman, J. T., Stewart, A. R., Kim, E., Baumann, Z., Kim, J.-H., & Manceau, A. (2021). Isotope Fractionation from *In Vivo* Methylmercury Detoxification in Waterbirds. *ACS Earth and Space Chemistry*, *5*(5), 990–997. https://doi.org/10.1021/acsearthspacechem.1c00051

Qian, J., Skyllberg, U., Tu, Q., Bleam, W. F., & Frech, W. (2000). Efficiency of solvent extraction methods for the determination of methyl mercury in forest soils. *Fresenius' Journal of Analytical Chemistry*, *367*(5), 467–473. https://doi.org/10.1007/s002160000364

Qin, C., Chen, M., Yan, H., Shang, L., Yao, H., Li, P., & Feng, X. (2018). Compound specific stable isotope determination of methylmercury in contaminated soil. *Science of The Total Environment*, *644*, 406–412. https://doi.org/10.1016/j.scitotenv.2018.06.328

Qin, C., Du, B., Yin, R., Meng, B., Fu, X., Li, P., Zhang, L., & Feng, X. (2020). Isotopic Fractionation and Source Appointment of Methylmercury and Inorganic Mercury in a Paddy Ecosystem. *Environmental Science & Technology*, *54*(22), 14334–14342. https://doi.org/10.1021/acs.est.0c03341

Queipo-Abad, S., Rodríguez-González, P., & García Alonso, J. I. (2019). Measurement of compound-specific Hg isotopic composition in narrow transient signals by gas chromatography coupled to multicollector ICP-MS. *Journal of Analytical Atomic Spectrometry*, *34*(4), 753–763. https://doi.org/10.1039/C8JA00453F

Reinfelder, J. R., & Janssen, S. E. (2019). Tracking legacy mercury in the Hackensack River estuary using mercury stable isotopes. *Journal of Hazardous Materials*, *375*, 121–129. https://doi.org/10.1016/j.jhazmat.2019.04.074

Rodríguez-González, P., Epov, V. N., Pecheyran, C., Amouroux, D., & Donard, O. F. X. (2012). Species-specific stable isotope analysis by the hyphenation of chromatographic techniques with MC-ICPMS. *Mass Spectrometry Reviews*, *31*(4), 504–521. https://doi.org/10.1002/mas.20352

Rosera, T. J., Janssen, S. E., Tate, M. T., Lepak, R. F., Ogorek, J. M., DeWild, J. F., Babiarz, C. L., Krabbenhoft, D. P., & Hurley, J. P. (2020). Isolation of methylmercury using distillation and anion-exchange chromatography for isotopic analyses in natural matrices. *Analytical and Bioanalytical Chemistry*, *412*(3), 681–690. https://doi.org/10.1007/s00216-019-02277-0

Russell, W. A., Papanastassiou, D. A., & Tombrello, T. A. (1978). Ca isotope fractionation on the Earth and other solar system materials. *Geochimica et Cosmochimica Acta*, *42*(8), 1075–1090. https://doi.org/10.1016/0016-7037(78)90105-9

Schaefer, J. K., Yagi, J., Reinfelder, J. R., Cardona, T., Ellickson, K. M., Tel-Or, S., & Barkay, T. (2004). Role of the Bacterial Organomercury Lyase (MerB) in Controlling Methylmercury Accumulation in Mercury-Contaminated Natural Waters. *Environmental Science & Technology*, *38*(16), 4304–4311. https://doi.org/10.1021/es049895w

Schauble, E. A. (2004). Applying Stable Isotope Fractionation Theory to New Systems. *Reviews in Mineralogy and Geochemistry*, *55*(1), 65–111. https://doi.org/10.2138/gsrmg.55.1.65

Schuster, P. F., Schaefer, K. M., Aiken, G. R., Antweiler, R. C., Dewild, J. F., Gryziec, J. D., Gusmeroli, A., Hugelius, G., Jafarov, E., Krabbenhoft, D. P., Liu, L., Herman-Mercer, N., Mu, C., Roth, D. A., Schaefer, T., Striegl, R. G., Wickland, K. P., & Zhang, T. (2018). Permafrost Stores a Globally Significant Amount of Mercury. *Geophysical Research Letters*, *45*(3), 1463–1471. https://doi.org/10.1002/2017GL075571

Selin, N. E. (2009). Global Biogeochemical Cycling of Mercury: A Review. *Annual Review of Environment and Resources*, *34*(1), 43–63. https://doi.org/10.1146/annurev.environ.051308.084314

Sellers, P., Kelly, C. A., & Rudd, J. W. M. (2001). Fluxes of methylmercury to the water column of a drainage lake: The relative importance of internal and external sources. *Limnology and Oceanography*, *46*(3), 623–631. https://doi.org/10.4319/lo.2001.46.3.0623

Steffen, A., Douglas, T., Amyot, M., Ariya, P., Aspmo, K., Berg, T., Bottenheim, J., Brooks, S., Cobbett, F., Dastoor, A., Dommergue, A., Ebinghaus, R., Ferrari, C., Gardfeldt, K., Goodsite, M. E., Lean, D., Poulain, A. J., Scherz, C., Skov, H., … Temme, C. (2008). A synthesis of atmospheric mercury depletion event chemistry in the atmosphere and snow. *Atmospheric Chemistry and Physics*, *8*(6), 1445–1482. https://doi.org/10.5194/acp-8-1445-2008

Stein, E. D., Cohen, Y., & Winer, A. M. (1996). Environmental distribution and transformation of mercury compounds. *Critical Reviews in Environmental Science and Technology*, *26*(1), 1–43. https://doi.org/10.1080/10643389609388485

Štrok, M., Baya, P. A., Dietrich, D., Dimock, B., & Hintelmann, H. (2019). Mercury speciation and mercury stable isotope composition in sediments from the Canadian Arctic Archipelago. *Science of The Total Environment*, *671*, 655–665. https://doi.org/10.1016/j.scitotenv.2019.03.424

Sutherland, W. J., Broad, S., Butchart, S. H. M., Clarke, S. J., Collins, A. M., Dicks, L. V., Doran, H., Esmail, N., Fleishman, E., Frost, N., Gaston, K. J., Gibbons, D. W., Hughes, A. C., Jiang, Z., Kelman, R., LeAnstey, B., Le Roux, X., Lickorish, F. A., Monk, K. A., … Ockendon, N. (2019). A Horizon Scan of Emerging Issues for Global Conservation in 2019. *Trends in Ecology & Evolution*, *34*(1), 83–94. https://doi.org/10.1016/j.tree.2018.11.001

Tang, W., Chu, J., & Zhong, H. (2023). Alkaline extraction: An optimal approach for extracting methylmercury from paddy soils. *Science of The Total Environment*, *885*(Complete). https://doi.org/10.1016/j.scitotenv.2023.163776

Tarbier, B., Hugelius, G., Kristina Sannel, A. B., Baptista-Salazar, C., & Jonsson, S. (2021). Permafrost Thaw Increases Methylmercury Formation in Subarctic Fennoscandia. *Environmental Science & Technology*, *55*(10), 6710–6717. https://doi.org/10.1021/acs.est.0c04108

Thera, J. C., Kidd, K. A., Stewart, A. R., Bertolo, R. F., & O'Driscoll, N. J. (2022). Using tissue cysteine to predict the trophic transfer of methylmercury and selenium in lake food webs. *Environmental Pollution*, *311*, 119936. https://doi.org/10.1016/j.envpol.2022.119936

Tong, M., Yu, J., Liu, M., Li, Z., Wang, L., Yin, C., Ren, A., Chen, L., & Jin, L. (2021). Total mercury concentration in placental tissue, a good biomarker of prenatal mercury exposure, is associated with risk for neural tube defects in offspring.

Environment International, *150*, 106425. https://doi.org/10.1016/j.envint.2021.106425

Tsui, M. T. K., Blum, J. D., Kwon, S. Y., Finlay, J. C., Balogh, S. J., & Nollet, Y. H. (2012). Sources and Transfers of Methylmercury in Adjacent River and Forest Food Webs. *Environmental Science & Technology*, *46*(20), 10957–10964. https://doi.org/10.1021/es3019836

Tsui, M. T.-K., Blum, J. D., & Kwon, S. Y. (2020). Review of stable mercury isotopes in ecology and biogeochemistry. *Science of The Total Environment*, *716*, 135386. https://doi.org/10.1016/j.scitotenv.2019.135386

Tukhmetova, D., Lisec, J., Vogl, J., & Meermann, B. (2022). Data processing made easy: Standalone tool for automated calculation of isotope ratio from transient signals – IsoCor. *Journal of Analytical Atomic Spectrometry*, *37*(11), 2401–2409. https://doi.org/10.1039/D2JA00208F

Vieira, H. C., Morgado, F., Soares, A. M. V. M., & Abreu, S. N. (2015). Fish consumption recommendations to conform to current advice in regard to mercury intake. *Environmental Science and Pollution Research*, *22*(13), 9595–9602. https://doi.org/10.1007/s11356-015-4635-z

Wang, Y., Bartov, G., Wang, T., Reinfelder, J. R., Johnson, T. M., & Yee, N. (2021). Rapid Attainment of Isotopic Equilibrium after Mercury Reduction by Ferrous Iron Minerals and Isotopic Exchange between Hg(II) and Hg(0). *ACS Earth and Space Chemistry*, *5*(6), 1384–1394. https://doi.org/10.1021/acsearthspacechem.1c00026

Weber, J. H. (1993). Review of possible paths for abiotic methylation of mercury(II) in the aquatic environment. *Chemosphere*, *26*(11), 2063–2077. https://doi.org/10.1016/0045-6535(93)90032-Z

West, J., Babi, D., Azaroff, A., & Jonsson, S. (2023). Dimethylmercury in natural waters—Analytical and experimental considerations. *Limnology and Oceanography: Methods*, *21*(12), 837–846. https://doi.org/10.1002/lom3.10586

Whalin, L., Kim, E.-H., & Mason, R. (2007). Factors influencing the oxidation, reduction, methylation and demethylation of mercury species in coastal waters. *Marine Chemistry*, *107*(3), 278–294. https://doi.org/10.1016/j.marchem.2007.04.002

Wiederhold, J. G. (2015). Metal Stable Isotope Signatures as Tracers in Environmental Geochemistry. *Environmental Science & Technology*, *49*(5), 2606–2624. https://doi.org/10.1021/es504683e

Wiederhold, J. G., Cramer, C. J., Daniel, K., Infante, I., Bourdon, B., & Kretzschmar, R. (2010). Equilibrium Mercury Isotope Fractionation between Dissolved Hg(II) Species and Thiol-Bound Hg. *Environmental Science & Technology*, *44*(11), 4191–4197. https://doi.org/10.1021/es100205t

Xie, Q., LuPresent Address: ChemTrace Corpor, S., Evans, D., Dillon, P., & Hintelmann, H. (2005). High precision Hg isotope analysis of environmental samples using gold trap-MC-ICP-MS. *Journal of Analytical Atomic Spectrometry*, *20*(6), 515. https://doi.org/10.1039/b418258h

Yang, L., & Sturgeon, R. E. (2003). Comparison of mass bias correction models for the examination of isotopic composition of mercury using sector field ICP-MS. *Journal of Analytical Atomic Spectrometry*, *18*(12), 1452. https://doi.org/10.1039/b307973b

Yang, Z., Fang, W., Lu, X., Sheng, G.-P., Graham, D. E., Liang, L., Wullschleger, S. D., & Gu, B. (2016). Warming increases methylmercury production in an Arctic soil. *Environmental Pollution*, *214*, 504–509. https://doi.org/10.1016/j.envpol.2016.04.069

Yin, R., Feng, X., Chen, B., Zhang, J., Wang, W., & Li, X. (2015). Identifying the Sources and Processes of Mercury in Subtropical Estuarine and Ocean Sediments Using Hg Isotopic Composition. *Environmental Science & Technology*, *49*(3), 1347–1355. https://doi.org/10.1021/es504070y

Yuan, S., Zhang, Y., Chen, J., Kang, S., Zhang, J., Feng, X., Cai, H., Wang, Z., Wang, Z., & Huang, Q. (2015). Large Variation of Mercury Isotope Composition During a Single Precipitation Event at Lhasa City, Tibetan Plateau, China. *Procedia Earth and Planetary Science*, *13*, 282–286. https://doi.org/10.1016/j.proeps.2015.07.066

Zadnik, M. G., Specht, S., & Begemann, F. (1989). Revised isotopic composition of terrestrial mercury. *International Journal of Mass Spectrometry and Ion Processes*, *89*(1), 103–110. https://doi.org/10.1016/0168-1176(89)85035-9

Zhang, L., Yin, Y., Li, Y., & Cai, Y. (2022). Mercury isotope fractionation during methylmercury transport and transformation: A review focusing on analytical method, fractionation characteristics, and its application. *Science of The Total Environment*, *841*, 156558. https://doi.org/10.1016/j.scitotenv.2022.156558

Zhang, W., Sun, G., Yin, R., Feng, X., Yao, Z., Fu, X., & Shang, L. (2021). Separation of methylmercury from biological samples for stable isotopic analysis. *Journal of Analytical Atomic Spectrometry*, *36*(11), 2415–2422. https://doi.org/10.1039/D1JA00236H

Zheng, W., & Hintelmann, H. (2009). Mercury isotope fractionation during photoreduction in natural water is controlled by its Hg/DOC ratio. *Geochimica et Cosmochimica Acta*, *73*(22), 6704–6715. https://doi.org/10.1016/j.gca.2009.08.016

Zheng, W., & Hintelmann, H. (2010). Nuclear Field Shift Effect in Isotope Fractionation of Mercury during Abiotic Reduction in the Absence of Light. *The Journal of Physical Chemistry A*, *114*(12), 4238–4245. https://doi.org/10.1021/jp910353y

Zhou, Z., Tang, Z., Wang, H., Liu, K., Wang, Y., Xiao, X., Yin, Y., Liu, G., Cai, Y., & Li, Y. (2024). Spatial and temporal variations in the pollution status and sources of mercury in the Jiaozhou bay. *Environmental Pollution*, *346*, 123554. https://doi.org/10.1016/j.envpol.2024.123554

Appendix

List of Figures

Table S - 1. Recovery of inorganic mercury from anion exchange resin, eluted using L-cysteine.

Sample	Recovery of Hg (%)
Elusion #1	97.4
Elusion #2	105.5
Elusion #3	95.0
Average	99.3

Table S - 2. Recovery of MMHg in sample passed through anion exchange resin with different elusion volumes.

Elusion Volume (mL)	Recovery of MMHg (%)	SD	n
0	69.8	1.0	2
5	87.7	1.4	2
10	106.6	7.5	2
15	99.9	1.5	2
20	103.8	1.6	2
25	105.8	5.8	2
30	106.9	1.9	2
35	101.6	0.4	2

Table S - 3. Isotopic composition of MMHg passed through the resin compared to stock MMHg analysed directly.

Sample	n	δ^{204}	2SD	δ^{202}	2SD	δ^{201}	2SD	δ^{200}	2SD	δ^{199}	2SD
Resin	4	–1.72	0.09	–1.16	0.04	–0.81	0.11	–0.53	0.06	–0.22	0.09
Stock MMHg	9	–1.70	0.14	–1.15	0.06	–0.82	0.06	–0.54	0.05	–0.20	0.03

Sample	Δ^{199}	2SD	Δ^{200}	2SD	Δ^{201}	2SD
Resin	0.07	0.09	0.05	0.05	0.06	0.08
Stock MMHg	0.09	0.02	0.04	0.04	0.04	0.03

Table S - 4. Recovery of MMHg from BCR 580 using alkaline extraction method.

Trial	Recovery of MMHg (%)
1	95.5
2	100.7
3	97.4

Table S - 5. Recovery of MMHg of alkaline extractant passed through anion exchange resin with and without pH adjustment to pH=1.

Sample	Recovery (%)	SD	n
Unadjusted pH	5.8	0.8	3
Adjusted pH	43.6	1.6	3

Table S - 6. Measured MMHg concentration extracted using traditional distillation with increasing masses of sediment.

Mass of Sediment (g)	Measured MMHg Conc. (ng/g)	SD	n
0.5	12.4	1.4	3
1	12.9	1.1	3
2	14.0	1.9	3
3	8.9	1.3	3

Table S - 7. Measured MMHg concentration of two in-house reference sediments extracted using modified distillation procedure.

Mass of sample (g)	Measured Conc. of Sediment 1 (ng/g)	SD	Measured Conc. of Sediment 2 (ng/g)	SD
0.5	12.6	0.4	42.6	2.0
1.0	13.9	1.5	43.6	4.9
2.0	14.0	2.0	41.5	2.1
3.0	13.1	1.4	42.2	0.1
4.0	13.5	1.4	42.2	1.4
5.0	12.4	1.0	40.8	4.2

Table S - 8. Isotopic compositions of distilled stock MMHg samples.

Sample	n	δ^{204}	2SD	δ^{202}	2SD	δ^{201}	2SD	δ^{200}	2SD	δ^{199}	2SD
Full Distillation	4	–1.71	0.14	–1.16	0.10	–0.84	0.10	–0.52	0.07	–0.19	0.07
First 20% Fraction	3	–1.77	0.13	–1.17	0.09	–0.79	0.13	–0.54	0.07	–0.17	0.03
Second 20% Fraction	3	–1.72	0.07	–1.20	0.05	–0.85	0.09	–0.58	0.08	–0.21	0.05
Third 20% Fraction	3	–1.74	0.07	–1.15	0.08	–0.81	0.04	–0.53	0.03	–0.21	0.05
Fourth 20% Fraction	3	–1.62	0.28	–1.18	0.11	–0.85	0.11	–0.51	0.05	–0.19	0.03
Stock MMHg	9	–1.70	0.14	–1.15	0.06	–0.82	0.06	–0.54	0.05	–0.20	0.03

Sample	Δ^{199}	2SD	Δ^{200}	2SD	Δ^{201}	2SD
Full Distillation	0.10	0.06	0.06	0.03	0.03	0.05
First 20% Fraction	0.12	0.01	0.05	0.06	0.09	0.00
Second 20% Fraction	0.09	0.04	0.02	0.05	0.05	0.07
Third 20% Fraction	0.08	0.04	0.05	0.03	0.06	0.06
Fourth 20% Fraction	0.11	0.03	0.08	0.10	0.03	0.05
Stock MMHg	0.09	0.02	0.04	0.04	0.04	0.03

Table S - 9. Measured isotopic compositions of MMHg in BCR 464 reported in literature compared to ratios measured in this research.

Reference	n	δ^{204}	2SD	δ^{202}	2SD	δ^{201}	2SD	δ^{200}	2SD	δ^{199}	2SD
Bouchet et al. (2018)	6	0.86	0.24	0.70	0.11	2.49	0.05	0.43	0.08	2.49	0.09
Epov et al. (2008)	3			0.93	0.67	2.85	0.51	0.61	0.54	2.44	0.87
Epov et al. (2008)	3			0.65	0.30	2.61	0.48	0.38	0.36	2.69	0.43
Epov et al. (2010)	not reported	0.93	0.61	0.55	0.24	2.38	0.19	0.37	0.04	2.52	0.09
Masbou et al. (2013)	6			0.62	0.13	2.35	0.17	0.39	0.09	2.50	0.13
This work	8	0.87	0.11	0.70	0.09	2.40	0.09	0.48	0.10	2.46	0.11

Reference	Δ^{199}	2SD	Δ^{200}	2SD	Δ^{201}	2SD
Bouchet et al. (2018)	2.32	0.06	0.08	0.06	1.96	0.12
Epov et al. (2008)	2.21	0.07	0.14	0.24	2.15	0.07
Epov et al. (2008)	2.52	0.44	0.05	0.46	2.11	0.46
Epov et al. (2010)	2.41	0.15	0.10	0.08	1.97	0.26
Masbou et al. (2013)	2.34	0.11	0.08	0.05	1.88	0.07
This work	2.28	0.11	0.13	0.08	1.87	0.08

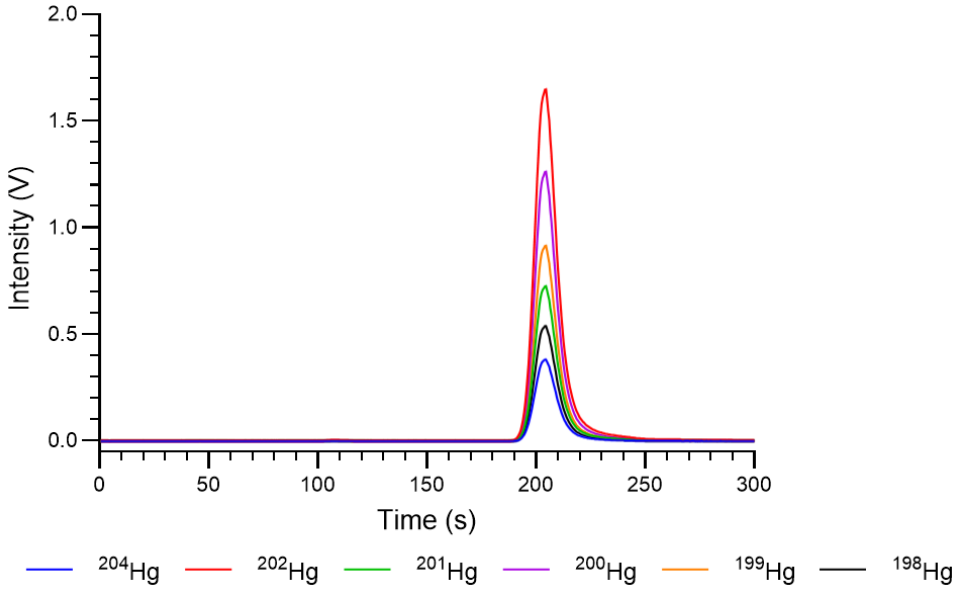

Figure S - 1. Chromatogram of NIST 3133.

Table S - 10. Isotope ratios calculated from NIST 3177 transient peak using SNIP baseline estimation method.

Ratio method	Zone [%]	δ^{204}	2SD	δ^{202}	2SD	δ^{201}	2SD	δ^{200}	2SD	δ^{199}	2SD
LRS	50	–0.63	3.35	0.74	3.89	–1.63	4.35	–0.70	3.43	3.43	6.87
LRS	60	–0.60	1.98	0.68	2.58	–1.01	3.80	–0.52	3.06	3.06	6.11
LRS	70	–0.42	1.19	0.19	2.40	–0.99	3.00	–0.38	2.29	2.29	4.57
LRS	80	–0.83	1.52	–0.29	1.80	–1.01	2.23	–0.50	2.27	2.27	4.54
LRS	90	–0.78	0.90	–0.37	1.26	–0.83	1.68	–0.41	1.77	1.77	3.55
LRS	95	–0.76	0.70	–0.44	0.97	–0.77	1.41	–0.41	1.53	1.53	3.06
LRS	100	–0.80	0.55	–0.51	0.76	–0.67	1.09	–0.39	1.24	1.24	2.48
PAI	50	–0.70	0.42	–0.56	0.76	–0.63	0.91	–0.38	1.19	1.19	2.37
PAI	60	–0.71	0.42	–0.64	0.65	–0.65	0.77	–0.40	1.07	1.07	2.14
PAI	70	–0.76	0.44	–0.65	0.58	–0.64	0.69	–0.41	1.01	1.01	2.02
PAI	80	–0.68	0.41	–0.61	0.61	–0.59	0.71	–0.38	0.89	0.89	1.79
PAI	90	–0.67	0.47	–0.62	0.57	–0.59	0.62	–0.40	0.85	0.85	1.70
PAI	95	–0.64	0.49	–0.63	0.59	–0.59	0.57	–0.40	0.81	0.81	1.62
PAI	100	–0.52	0.60	–0.66	0.62	–0.64	0.45	–0.41	0.79	0.79	1.58
PBP	50	–0.80	0.71	–0.49	0.84	–0.48	0.43	–0.75	1.47	1.47	2.94
PBP	60	–0.80	0.70	–0.59	0.47	–0.46	0.50	–0.66	0.77	0.77	1.54
PBP	70	–0.86	0.81	–0.61	0.57	–0.46	0.54	–0.62	1.13	1.13	2.27
PBP	80	–0.73	0.55	–0.59	0.82	–0.46	0.62	–0.58	1.05	1.05	2.10
PBP	90	–0.63	0.72	–0.76	0.90	–0.52	0.51	–0.62	0.79	0.79	1.57
PBP	95	–0.47	0.97	–0.85	1.16	–0.52	0.45	–0.54	0.68	0.68	1.36
PBP	100	0.17	0.70	–0.97	1.16	–0.82	0.72	–0.52	0.84	0.84	1.67
Certified Values		–0.82	0.07	–0.56	0.03	–0.46	0.02	–0.27	0.01	–0.17	0.01

Table S - 11. Isotope ratios calculated from NIST 3177 transient peak using TopHat baseline estimation method.

Ratio method	Zone [%]	δ^{204}	2SD	δ^{202}	2SD	δ^{201}	2SD	δ^{200}	2SD	δ^{199}	2SD
LRS	50	0.60	3.63	0.68	3.88	–1.80	4.41	–0.68	3.28	1.48	1.56
LRS	60	–0.61	2.16	0.65	2.55	–1.14	3.71	–0.55	3.07	1.48	0.92
LRS	70	–0.39	1.31	0.20	2.35	–0.99	2.99	–0.38	2.29	1.01	0.97
LRS	80	–0.77	1.61	–0.27	1.81	–1.01	2.23	–0.49	2.26	0.61	1.38
LRS	90	–0.76	1.07	–0.38	1.28	–0.84	1.67	–0.41	1.77	0.46	0.94
LRS	95	–0.74	0.85	–0.44	0.98	–0.77	1.41	–0.41	1.54	0.39	0.78
LRS	100	–0.78	0.70	–0.52	0.76	–0.66	1.07	–0.39	1.24	0.33	0.53
PAI	50	–0.76	0.54	–0.52	0.72	–0.59	1.05	–0.33	1.34	0.30	0.45
PAI	60	–0.78	0.60	–0.60	0.60	–0.60	0.90	–0.35	1.23	0.22	0.46
PAI	70	–0.83	0.57	–0.61	0.57	–0.60	0.86	–0.36	1.20	0.21	0.48
PAI	80	–0.78	0.44	–0.57	0.59	–0.55	0.90	–0.33	1.13	0.24	0.35
PAI	90	–0.77	0.51	–0.57	0.61	–0.54	0.88	–0.32	1.15	0.24	0.44
PAI	95	–0.79	0.54	–0.56	0.64	–0.52	0.88	–0.31	1.18	0.24	0.51
PAI	100	–0.77	0.97	–0.54	0.93	–0.51	1.11	–0.26	1.54	0.23	0.92
PBP	50	–0.87	0.81	–0.44	0.73	–0.43	0.50	–0.66	1.60	0.06	0.58
PBP	60	–0.86	0.73	–0.50	0.51	–0.43	0.54	–0.60	1.06	0.00	0.75
PBP	70	–0.93	0.79	–0.60	0.71	–0.41	0.64	–0.53	1.50	0.03	0.84
PBP	80	–0.81	0.50	–0.57	1.02	–0.42	0.79	–0.50	1.43	0.07	0.69
PBP	90	–0.75	0.76	–0.61	1.22	–0.42	0.78	–0.42	1.39	0.11	0.47
PBP	95	–0.79	1.06	–0.59	1.35	–0.38	0.88	–0.32	1.36	0.24	0.84
PBP	100	–0.93	4.17	–0.44	3.60	–0.24	2.36	0.08	4.71	0.32	3.80
Certified Values		–0.82	0.07	–0.56	0.03	–0.46	0.02	–0.27	0.01	–0.17	0.01

Table S - 12. Isotope ratios calculated from NIST 3177 transient peak using ConvexHull baseline estimation method.

Ratio method	Zone [%]	δ^{204}	2SD	δ^{202}	2SD	δ^{201}	2SD	δ^{200}	2SD	δ^{199}	2SD
LRS	50	–0.60	3.44	0.74	3.89	–1.63	4.35	–0.70	3.44	1.51	1.61
LRS	60	–0.58	2.05	0.68	2.58	–1.01	3.80	–0.52	3.06	1.51	0.88
LRS	70	–0.39	1.32	0.19	2.40	–0.99	3.00	–0.38	2.29	1.02	0.93
LRS	80	–0.80	1.61	–0.29	1.80	–1.01	2.23	–0.50	2.27	0.60	1.40
LRS	90	–0.75	1.08	–0.37	1.26	–0.83	1.68	–0.41	1.78	0.46	0.92
LRS	95	–0.74	0.86	–0.44	0.97	–0.77	1.41	–0.41	1.53	0.39	0.76
LRS	100	–0.77	0.71	–0.51	0.76	–0.67	1.10	–0.39	1.24	0.33	0.54
PAI	50	–0.60	0.49	–0.55	0.75	–0.61	0.91	–0.37	1.21	0.29	0.48
PAI	60	–0.61	0.49	–0.63	0.65	–0.64	0.77	–0.39	1.10	0.20	0.53
PAI	70	–0.65	0.48	–0.64	0.57	–0.62	0.69	–0.40	1.04	0.20	0.47
PAI	80	–0.56	0.41	–0.59	0.58	–0.57	0.70	–0.37	0.91	0.24	0.30
PAI	90	–0.53	0.34	–0.61	0.54	–0.57	0.61	–0.38	0.87	0.23	0.28
PAI	95	–0.48	0.31	–0.61	0.55	–0.55	0.54	–0.38	0.84	0.23	0.27
PAI	100	–0.24	0.36	–0.63	0.55	–0.57	0.41	–0.39	0.83	0.23	0.30
PBP	50	–0.69	0.61	–0.48	0.85	–0.45	0.44	–0.74	1.50	0.03	0.67
PBP	60	–0.69	0.58	–0.59	0.43	–0.44	0.51	–0.65	0.80	–0.02	0.80
PBP	70	–0.76	0.65	–0.60	0.51	–0.44	0.54	–0.60	1.15	0.04	0.84
PBP	80	–0.62	0.29	–0.56	0.71	–0.44	0.61	–0.57	1.01	0.10	0.69
PBP	90	–0.52	0.38	–0.77	0.81	–0.48	0.52	–0.63	0.67	0.08	0.40
PBP	95	–0.31	0.60	–0.83	1.19	–0.47	0.43	–0.53	0.61	0.05	0.48
PBP	100	1.50	1.79	–0.66	0.82	–0.71	0.79	–0.38	1.44	0.31	1.65
Certified Values		–0.82	0.07	–0.56	0.03	–0.46	0.02	–0.27	0.01	–0.17	0.01

Table S - 13. Isotope ratios calculated from NIST 3177 transient peak using Median baseline estimation method.

Ratio method	Zone [%]	δ^{204}	2SD	δ^{202}	2SD	δ^{201}	2SD	δ^{200}	2SD	δ^{199}	2SD
LRS	50	–0.58	3.61	0.68	3.89	–1.80	4.41	–0.68	3.28	1.48	1.57
LRS	60	–0.69	1.79	0.66	2.63	–1.31	3.98	–0.51	2.92	1.47	0.72
LRS	70	–0.27	1.38	0.32	2.39	–0.91	2.81	–0.37	2.51	1.15	1.18
LRS	80	–0.70	1.63	–0.25	1.78	–0.99	2.30	–0.47	2.26	0.64	1.43
LRS	90	–0.75	1.12	–0.38	1.29	–0.86	1.73	–0.42	1.82	0.47	1.00
LRS	95	–0.74	0.93	–0.43	1.03	–0.78	1.46	–0.42	1.57	0.40	0.82
LRS	100	–0.78	0.77	–0.51	0.79	–0.69	1.13	–0.40	1.32	0.34	0.59
PAI	50	–0.79	0.36	–0.49	0.74	–0.61	1.23	–0.28	1.22	0.38	0.37
PAI	60	–0.79	0.40	–0.57	0.61	–0.62	1.09	–0.29	1.12	0.31	0.41
PAI	70	–0.89	0.46	–0.60	0.52	–0.64	1.08	–0.30	1.07	0.28	0.38
PAI	80	–0.82	0.32	–0.54	0.66	–0.59	1.13	–0.26	1.01	0.33	0.43
PAI	90	–0.82	0.43	–0.53	0.69	–0.57	1.15	–0.25	1.01	0.35	0.55
PAI	95	–0.83	0.55	–0.53	0.75	–0.57	1.21	–0.22	1.03	0.37	0.63
PAI	100	–0.85	0.91	–0.48	0.89	–0.59	1.48	–0.17	1.18	0.43	0.95
PBP	50	–0.92	0.71	–0.40	0.71	–0.44	0.66	–0.62	1.43	0.12	0.58
PBP	60	–0.88	0.63	–0.44	0.54	–0.45	0.65	–0.58	1.05	0.08	0.71
PBP	70	–1.03	0.72	–0.57	0.64	–0.47	0.77	–0.53	1.19	0.11	0.73
PBP	80	–0.90	0.41	–0.56	1.17	–0.44	0.98	–0.41	1.55	0.20	0.76
PBP	90	–0.80	0.70	–0.60	1.26	–0.39	0.90	–0.26	1.70	0.28	0.75
PBP	95	–0.80	1.05	–0.71	1.70	–0.44	1.19	–0.01	1.63	0.42	1.39
PBP	100	–0.61	3.08	–0.27	3.16	–0.59	2.64	0.17	3.38	0.90	4.05
Certified Values		–0.82	0.07	–0.56	0.03	–0.46	0.02	–0.27	0.01	–0.17	0.01

Table S - 14. Comparison of integration time on stock MMHg isotopic composition calculated using PAI of 80% of the peak with TopHat baseline estimation method.

Sample	n	δ^{204}	2SD	δ^{202}	2SD	δ^{201}	2SD	δ^{200}	2SD	δ^{199}	2SD
0.5 sec int	3	–1.93	0.46	–1.55	1.59	–0.97	1.56	–0.90	2.00	–0.06	0.59
1 sec int	3	–1.67	0.60	–1.57	0.36	–0.59	0.87	–0.83	2.00	0.29	1.45
Stock MMHg	9	–1.70	0.14	–1.15	0.06	–0.82	0.06	–0.54	0.05	–0.20	0.03

Sample	Δ^{199}	2SD	Δ^{200}	2SD	Δ^{201}	2SD	Δ^{204}	2SD
0.5 sec int	0.32	0.40	–0.11	1.49	0.09	1.12	–0.87	0.39
1 sec int	0.74	1.58	–0.31	2.39	0.72	0.75	–0.46	0.74
Stock MMHg	0.09	0.02	0.04	0.04	0.04	0.03	0.03	0.05

Table S - 15. Average THg concentration of lakes in summer and winter.

	Winter		Summer	
	Conc. of THg (ng/g)	SD	Conc. of THg (ng/g)	SD
Lake 5	67.0	5.4	68.1	7.0
Lake 11	15.9	4.3	57.8	4.2
Lake 9	–		36.1	3.8

Table S - 16. Measures THg isotope ratios of sediment samples.

Sample	δ^{204}	δ^{202}	δ^{201}	δ^{200}	δ^{199}	Δ^{199}	Δ^{200}	Δ^{201}
L5NAT0 Winter	–1.71	–1.20	–1.30	–0.35	–0.54	–0.24	0.25	–0.39
L5NAT24 Winter	–1.71	–1.21	–1.30	–0.35	–0.54	–0.24	0.25	–0.39
L5L Winter	–1.71	–1.09	–1.23	–0.45	–0.62	–0.34	0.10	–0.41
L5S Winter	–1.73	–1.14	–1.22	–0.40	–0.60	–0.31	0.17	–0.37
L5L+S Winter	–1.66	–1.12	–1.20	–0.48	–0.62	–0.34	0.08	–0.36
L5NAT0 Summer	–1.45	–1.02	–1.10	–0.40	–0.56	–0.30	0.11	–0.33
L5NAT12 Summer	–1.42	–1.07	–1.11	–0.52	–0.56	–0.29	0.02	–0.31
L5L Summer	–1.32	–1.01	–1.10	–0.49	–0.57	–0.32	0.02	–0.34
L5S Summer	–1.33	–0.98	–1.12	–0.46	–0.55	–0.31	0.03	–0.38
L5L+S Summer	–1.54	–1.01	–1.15	–0.48	–0.61	–0.36	0.02	–0.39
L11NAT0 Winter	–2.13	–1.46	–1.29	–0.04	–0.56	–0.20	0.69	–0.19
L11NAT12 Winter	–2.07	–1.42	–1.24	–0.27	–0.53	–0.18	0.45	–0.17
L11L Winter	–2.25	–1.39	–1.31	–0.48	–0.52	–0.17	0.22	–0.26
L11S Winter	–2.22	–1.44	–1.29	–0.08	–0.56	–0.20	0.65	–0.21
L11L+S Winter	–2.15	–1.52	–1.31	–0.60	–0.58	–0.20	0.16	–0.16
L11NAT0 Summer	–1.85	–1.28	–1.34	–0.64	–0.69	–0.37	0.00	–0.38
L11NAT12 Summer	–1.89	–1.33	–1.32	–0.66	–0.54	–0.21	0.01	–0.32
L11L Summer	–1.77	–1.22	–1.26	–0.61	–0.64	–0.34	0.00	–0.34
L11S Summer	–2.01	–1.37	–1.38	–0.70	–0.69	–0.35	–0.01	–0.35
L11L+S Summer	–1.89	–1.30	–1.30	–0.64	–0.67	–0.34	0.02	–0.33
L9NAT0 Summer	–2.22	–1.56	–1.59	–0.77	–0.79	–0.40	0.01	–0.42
L9NAT12 Summer	–2.26	–1.56	–1.45	–0.76	–0.67	–0.27	0.02	–0.28
L9L Summer	–2.36	–1.61	–1.50	–0.81	–0.68	–0.27	0.00	–0.29
L9S Summer	–2.15	–1.46	–1.55	–0.73	–0.83	–0.47	0.00	–0.45
L9L+S Summer	–2.06	–1.41	–1.35	–0.72	–0.60	–0.24	–0.01	–0.29

Table S - 17. Measured MMHg isotope ratio from sediment samples calculated using PAI of 80% of the peak with TopHat baseline estimation method.

Sample	n	δ^{204}	2SD	δ^{202}	2SD	δ^{201}	2SD	δ^{200}	2SD	δ^{199}	2SD
L5 NA T0 Summer	3	–1.14	3.68	–2.35	2.00	–1.17	1.87	–0.38	3.10	–0.20	1.13
L5 NA T12 Summer	3	–2.43	1.55	–3.20	0.74	–1.64	2.19	–1.71	0.40	–1.54	0.43
L5 S Summer	3	–1.41	3.50	–2.64	2.07	–1.92	1.96	–1.23	2.59	–0.97	2.59

Sample	Δ^{199}	2SD	Δ^{200}	2SD	Δ^{201}	2SD	Δ^{204}	2SD
L5 NA T0 Summer	0.39	1.04	0.80	2.12	0.59	2.57	2.36	0.74
L5 NA T12 Summer	–0.73	0.49	–0.10	0.25	0.77	2.59	2.35	2.06
L5 S Summer	–0.31	2.18	0.09	1.62	0.06	0.45	2.52	1.30